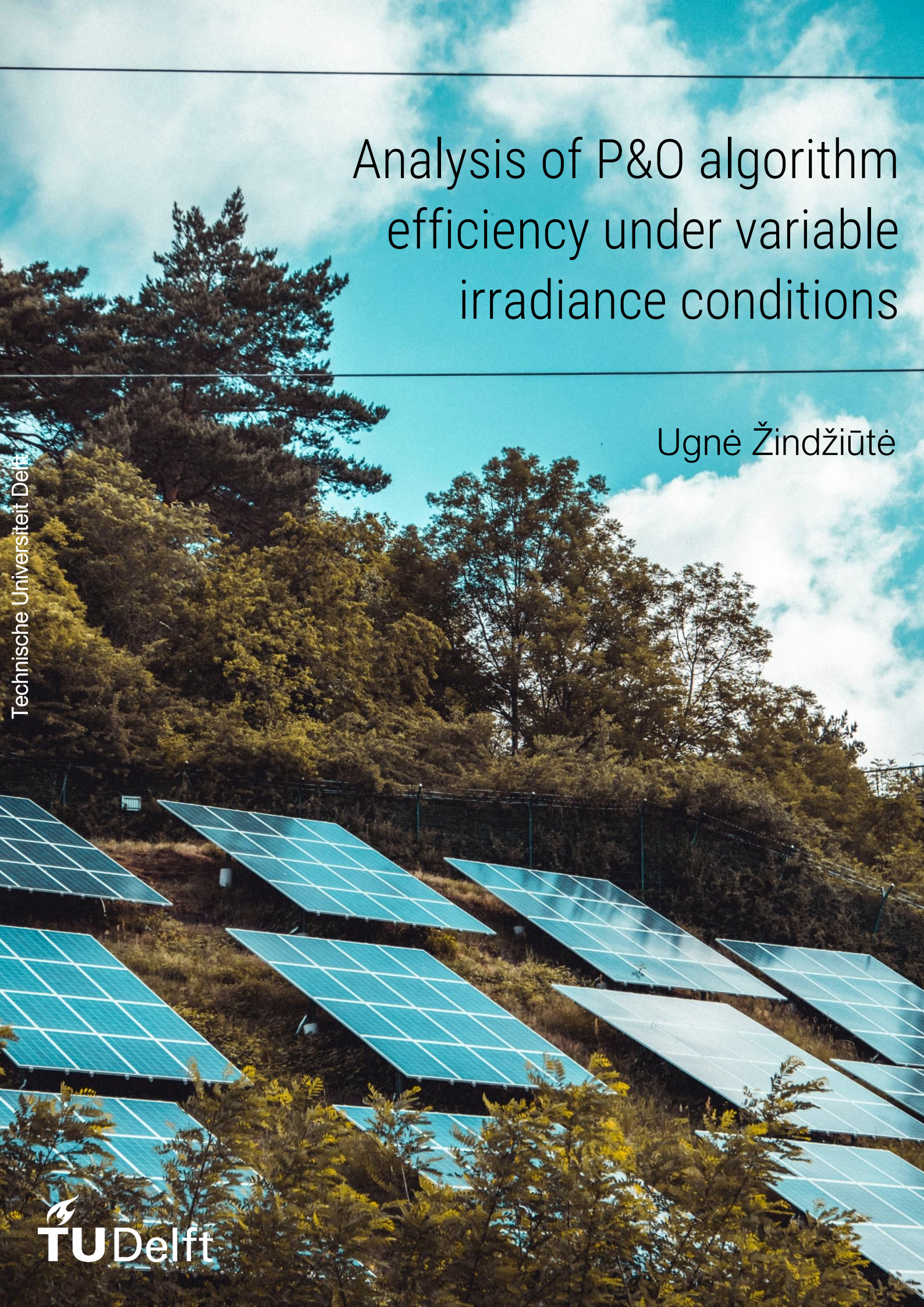

Analysis of P&O algorithm efficiency under variable irradiance conditions

Ugnė Žindžiūtė

Technische Universiteit Delft

TU Delft

Analysis of P&O algorithm efficiency under variable irradiance conditions

Master's thesis report

by

Ugnė Žindžiūtė

to obtain the degree of Master of Science in Sustainable Energy Technology
at the Delft University of Technology,
to be defended publicly on October 7, 2021.

Faculty of Electrical Engineering, Mathematics & Computer Science, Delft University of Technology

Student number:	5075483	
Project duration:	November 16, 2020 – October 7, 2021	
Thesis committee:	Prof. Dr. ir. Olindo Isabella,	TU Delft, head of PVMD group
	Dr. ir. Heasn Ziar,	TU Delft, PVMD, supervisor
	Dr. Aditya Shekhar,	TU Delft, DCES, external member
	Ir. Victor Arturo Martinez Lopez	TU Delft, PVMD, daily supervisor

An electronic version of this thesis is available at http://repository.tudelft.nl/.

TU Delft

Preface

In front of you lies the past 10 months of my honest work, my thesis to obtain a MSc Sustainable energy technology degree. Throughout the process of research presented in this report, I have encountered many challenges from not knowing where to start, to realizing the scope of work in its entirety, to not being able to release control and accept the imperfections in the work. It was most definitely difficult to overcome these obstacles and I had to push myself to the limit. However, by doing this I learned and experienced so much and the success I achieved now gives me a lot of joy. I have learned a lot from a professional side as well. I believe after completing this thesis I will be able to think more critically, creatively and solve problems by employing the extensive amount of knowledge this programme has provided me. Obtaining this degree will allow me to participate in the fight angainst climate change and energy transition to the best of my capabilities. Nonetheless, completing this thesis would not have been possible without the people I would like to thank.

Firstly, I would like to thank my daily supervisor Arturo Martinez Lopez for his patience, constant support and guidance. A lot of our work did not go to plan and I am glad that we have managed to agree and adjust to the situation. Furthermore, I am grateful to Dr. Hesan Ziar, the supervisor of this project. His critical thinking and observations about this thesis and its conclusions have improved the work immensely. Through the few meetings we had, he has challenged my point of view and lead to interesting findings. Lastly, I would like to thank Dr. Aditya Sherkhar and Prof. Dr. Olindo Isabella for taking the time to evaluate my work and discuss its contents during the defence.

I am extremely grateful to my parents for the constant support, listening to me nag about my frustrations and sending good words back. DETRA Solar leaders David and Justė also deserve a mention, without their understanding of my strive for knowledge I would not have been able to pursue it. I would like to also thank my new friends in Delft and old ones back home, these two years would not have been as much fun without them. Lastly, special appreciation goes to my best friend and partner Ayush for holding me together at my worst and dancing in joy at best.

And for the ones reading this thesis, I wish you a pleasant and informative read.

Ugnė Žindžiūtė
Delft, September 2021

Abstract

Fight against climate change is facilitated through energy transition which entails changing the fossil fuel based energy generation to sustainable resources such as solar PV. However, PV installations require extensive resources for their development and construction, so it is essential that the efficiency of energy conversion is high. A very important factor to ensure PV system efficiency is use of maximum power point tracking (MPPT). MPPT controls the system's operating point so that at each instance power drawn from a PV module or array is the maximum power available. This is realised by employing a DC-DC converter controlled by an MPPT algorithm. The most widely used algorithm due to its simplicity and cost of implementation is the Perturb and Observe (P&O) algorithm. However, its performance is not ideal in both steady-state and dynamic conditions. The algorithm's operation depends on the P&O parameters and conditions in which the algorithm operates are influenced by irradiance variability.

There are a number of studies on P&O algorithm efficiency and irradiance variability separately, however, a link between these two topics has not been explored. Thus, this thesis aims to bridge the gap and its purpose is to determine the relationship between P&O algorithm efficiency and irradiance variability. This was carried out by use of real 3-second irradiance data from Oahu, Hawaii, modelling the power output of a PV module and obtaining the operating point of the system by implementing a P&O algorithm without assuming any physical properties of a DC-DC converter. Then using operating point and maximum power point power values, 3 s averages of the P&O algorithm efficiency were computed, and variability metrics were calculated using the original irradiance data. Finally, an exploratory analysis of the prepared dataset was performed to determine how the P&O algorithm varies when exposed to different irradiance variability. Additionally, a sensitivity analysis was deemed necessary to examine efficiency dependence on P&O algorithm parameters - sampling interval and perturbation amplitude - in different cases of irradiance variability.

The results of this research have shown variations of P&O efficiency values on different time scales as well as in different variability conditions. Each day of the year was classified by occurring irradiance variability. It was confirmed that efficiency depends on the variability class of the day with the lowest efficiencies down to 99.8 % found for highly variable days. Monthly P&O efficiency was determined to be affected by the number of days from each class. P&O efficiency was highest when the least days in the month were classified as highly variable. Monthly efficiencies were found to be above 99.9 %. To describe the relationship between variability and P&O efficiency, variability metrics were selected and computed for 1 min periods. Major scattering of data was found when 1 min averaged efficiency was plotted against any of the variability metrics. Magnitudes of 1 min average efficiency was determined to be mostly above 95 %. To reduce scattering, average efficiencies that could be expected in bins of variability metrics were determined, and in such a case, a general decrease in efficiency was observed with increasing magnitudes of variability metrics. Additionally, polynomial fits through the data were produced to provide functions with which P&O efficiency could be approximated when variability described by a metric is known. Lastly, P&O efficiency sensitivity to its parameters study has shown that in most cases efficiency is more sensitive to perturbation amplitude, however, in high variability, sampling interval and perturbation amplitude must be sufficiently small ($\Delta V \leq 1\%$ of $V_{oc(STC)}$, $T_a \leq 10$ ms) for better performance of the algorithm.

List of Figures

List of Tables

Contents

Acronyms

AOI Angle of incidence.

CDF Cumulative distribution function.

DHI Direct horizontal irradiance.
DNI Direct normal irradiance.
DOY Day of year.

ESRA European Solar Radiation Atlas.

GHI Global horizontal irradiance.

HOMER Hybrid Optimization of Multiple Energy Resources.

IC Incremental conductance.

K-S Kolmogorov-Smirnov test.

MPP Maximum power point.
MPPT Maximum power point tracking.

OP Operating point.

P&O Perturb and observe.
PV Photo-voltaic.

RMSE Root mean squared error.
RSR Rotating shadowband radiometer.

STC Standard test conditions.
SVF Sky view factor.

VI Variability index.

1

Introduction

Climate change is one of the most important issues that humankind has to deal with these days. The effects of global warming are already felt around the globe with the increasing frequency of intense droughts that cause disasters like massive forest fires, floods and storms that destroy property and leave people without homes. To prevent the Earth from being inhabitable a lot of action is taken to reduce the increasing rate of such occurrences of catastrophic events. Climate change is caused by human activities during which greenhouse gases are released that traps the incoming Sun's energy inside the atmosphere which results in warming of the Earth. Most of these greenhouse gases (especially CO_2) is released when burning fossil fuels [1] and the highest source of greenhouse gasses is the energy sector [2]. Globally, most of the energy supply comes from fossil fuels [3] and hence energy transition is the most important way to fight climate change. Energy transition refers to a change of the source from which energy is generated from fossil fuels to sustainable resources such as wind, Sun and water. To achieve energy transition, more and more capacity of renewable generators is installed. Solar photo-voltaic (PV) installations in current years contribute to more than half of total installed renewable energy capacity [4] and hence can be considered as the leader of renewable energy sector.

Increasing solar PV installed capacity requires increasing resources such as land area, production and disposal of PV system components, finances and human resources. Therefore, it is essential for PV installations to produce as much energy as possible. For this, a lot of research efforts are put to increase efficiency of the PV system so that with the same resources more energy could be extracted. There are three main factors that limit PV system efficiency: (1) efficiency of energy conversion by the solar cell (up to ~23 % in commercial applications [5]), (2) efficiency of power converters (~95-98 %) and (3) efficiency of maximum power point tracking (MPPT) (~98 %) [6]. MPPT is done by use of an algorithm that governs operation of a power converter which can change voltage and current in the system. The goal of MPPT is to ensure that the operating voltage and current is such that the power extracted from the module is maximum at all times. This makes MPPT an essential part of the PV system. Also, implementation of improvements made in MPPT algorithms are much simpler and cheaper as they can be easily retrofitted into an existing PV system [6].

Researchers have made great efforts to improve MPPT by creating new algorithms or modifying existing ones. However, performance of the algorithm is related to its complexity and more complex algorithms are more costly to implement [7]. Hence, to this day one of the simplest of MPPT techniques - Perturb and Observe (P&O) algorithm - is most widely used in commercial applications and referred to in literature [7] [8] [9]. P&O algorithm controls the voltage of the system by perturbing - positively or negatively changing the operating voltage by a predefined step called perturbation amplitude ΔV - and observing whether the voltage change results in an increase or decrease in the power extracted from the PV module. The frequency of perturbations is determined by the sampling interval T_a, which together with ΔV is called P&O parameters. While the algorithm is simple and cheap, it also has some drawbacks. One of the main issues that P&O endures is the confusion and slow response during rapidly changing irradiance conditions. The severity of this issue is dependant on the parameters P&O is set to operate at. There is a methodology proposed to optimise the parameters so that performance of the algorithm would be adequate [8], but researches to investigate operation of the P&O algorithm are limited.

As mentioned before, P&O algorithm efficiency is affected by rapid changes of irradiance magnitude in literature referred to as irradiance variability. Change in irradiance happen due to Earth's movement around the Sun and its own axis, and, more importantly, by cloud formation and movement. Movement

of the Earth results in slow daily variations where irradiance values start rising from sunrise, peak at noon and descends until sunset, whereas fast-moving clouds induce the rapid changes in short time periods that are of interest when studying P&O performance. Research has focused greatly to quantify on-site variability by introducing metrics that would best describe the conditions of irradiance in temporal or/and spatial dimensions [10] [11] [12]. However, motivation for irradiance variability studies is mainly based on the necessity of understanding fluctuating PV power plant output [12]. This is of course very important to consider especially in cases where renewable energy sustains the majority of system load and fluctuations in power output can have severe repercussions. However, as irradiance variability influences not only the output but also performance of a PV power plant, variability of irradiance can be included in PV system components' performance research as well.

This thesis aims to bridge the gap between research on MPPT efficiency and irradiance variability, as well as deepen the understanding of P&O MPPT algorithm operation in real-world conditions. Consequently, the research question of this thesis is:

How does efficiency of maximum power point tracking P&O algorithm vary when exposed to different conditions of irradiance variability?

Sub-questions that aids to properly reason the answer to the main research question can be identified as follows:

- *Is there variation in daily and monthly efficiency of P&O algorithm, and if there is how can such variation be explained?*
- *How can variability be quantified? How do these quantities relate to efficiency?*
- *Does P&O parameter tuning have an influence on P&O efficiency? How does that depend on irradiance variability?*

The report of this thesis is sectioned as follows. Firstly, Chapter 2 presents concepts necessary to understand working principles of P&O algorithm. It also provides a literature review carried out throughout this project. Then the report moves on to explain the methodology undertaken to provide the results necessary for answering the aforementioned research question in Chapter 3. Results of the analysis done are presented in Chapter 4 which also provides a result-specific discussion. The general observations made in the process of the project are given and discussed in Chapter 5. Lastly, Chapter 6 summarises the thesis and provides recommendations for future work.

2

Literature review

Prior to performing active research to answer the questions proposed, a thorough literature review was done. This chapter aims to present the concepts necessary to understand maximum power point tracking as well as its importance, realisation and performance. Thus this chapter starts with Section 2.1 in which the PV module's power output and its changes are discussed. Section 2.2 talks about how the changes in PV output can be tracked to ensure maximum utilization of available power. Then Section 2.3 focuses on the P&O MPPT algorithm and its operation in steady as well as dynamic conditions. Additionally, the current state of existing literature is discussed to better understand the necessity and novelty of this thesis. Hence an overview of the studies on P&O efficiency is provided in Section 2.4. Also, Section 2.5 gives an introduction to irradiance variability research. Lastly, Section 2.6 summarises the contents of this chapter.

2.1 PV module output under changing irradiance

PV module being the solar to electrical energy converter relies on solar irradiance incident on the module to produce power. However, the power output drawn from a PV module depends on the current and voltage at which the solar generation system operates. PV modules have a distinguishable characteristic in terms of current versus voltage and power versus voltage as shown in Figure 2.1 [13]. These characteristic curves are dependant on the PV cells used to manufacture the module. The characteristic of a PV module only differs from PV cells' by the amplitude of the current (or power) and voltage subject to the interconnections between the cells [13]. The current versus voltage characteristic (or I-V curve) begins at short circuit current I_{sc} (when voltage is zero) and has a plateau before current starts to decrease down to open-circuit voltage V_{oc} (when current is zero). Since power is the product of current and voltage, the power versus voltage (or P-V curve) starts at zero and increases together with increasing voltage until a specific maximum power is reached and then drops to zero at V_{oc}. The maximum point of this curve is called the maximum power point (MPP). As is demonstrated in the Figure 2.2, the I-V and P-V curves depends on module operating temperature and irradiance [8]. With increasing irradiance, I-V curve shows a rise in the I_{sc} values as well as a narrower plateau which in consequence makes MPP take place at a lower voltage. On the other hand, an increase in temperature does not change I_{sc} but instead causes the V_{oc} to reduce which also results in maximum power point shift to lower voltage.

When a module is connected to a system the power drawn depends on the load. For example, if a load is a simple resistor, its I-V curve is a straight line as it follows I=V/R. This is demonstrated in Figure 2.3 which also shows two I-V curves of a PV module - one at higher irradiance (green curve) and one at lower (blue curve). The operating point (OP) of the overall system is the point at which the module and resistor I-V curves intersect [13]. Therefore, as seen in Figure 2.3, when irradiance is higher OP is equal to MPP which means that maximum power is drawn from the module. However, if the load does not change (i.e. when the load is a resistor with constant resistivity) but irradiance drops the intersection of the curves will not happen at MPP and OP will be at lower than maximum power. This results in loss of power output and in turn a decrease in system performance. Since such loss is not desirable it is necessary to force the system to operate at MPP. This is done by changing the operating voltage of the module using what is called MPP tracking (MPPT).

It is also important to note that the I-V and P-V curves seen in the figures exist under uniform

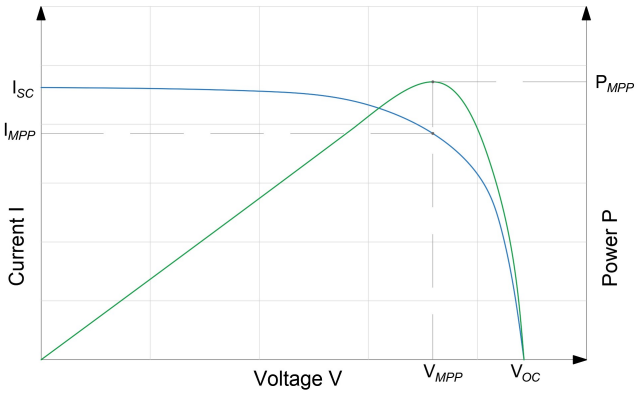

Figure 2.1: Generic I-V and corresponding P-V curve (adapted from [13])

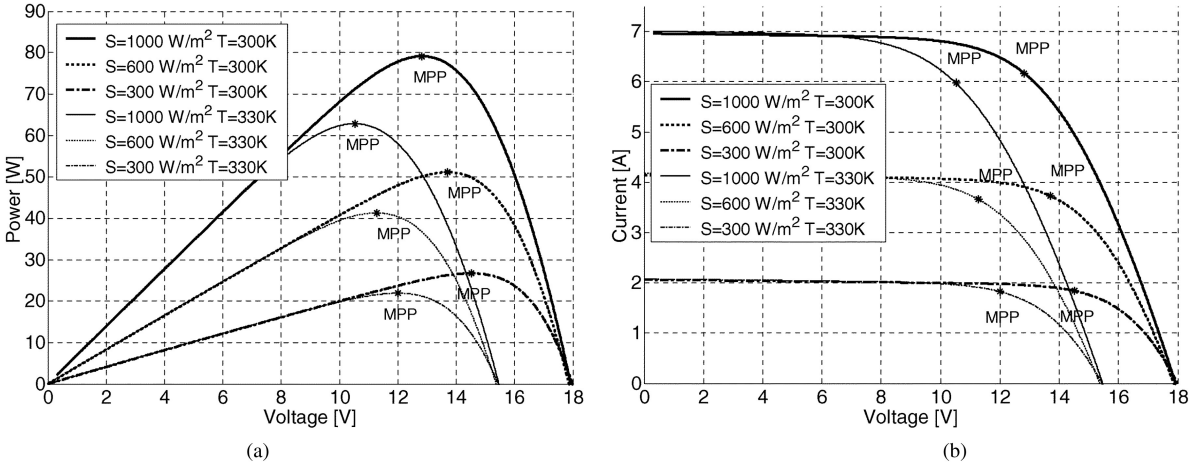

(a) (b)

Figure 2.2: (a) P-V and (b) I-V curves under different irradiance and temperature conditions [8]

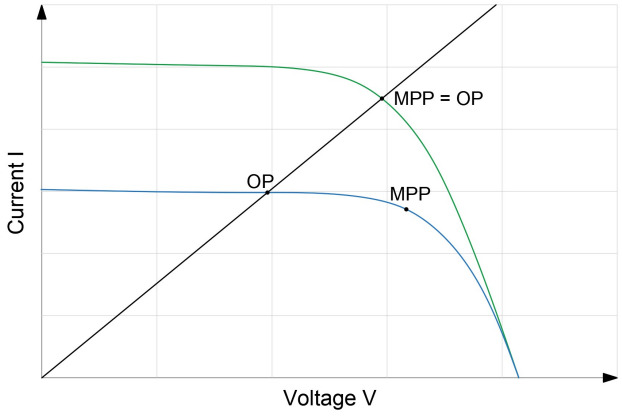

Figure 2.3: Operating points (OP) and maximum power point (MPP) under different irradiance (adapted from [13])

irradiance i.e. when the whole area of a module is illuminated equally. However, this is not always the case in real-world scenarios and partial shading of the module can happen when part of the module receives more irradiance than another. This causes a shaded region of the module to not generate, but dissipate energy and in turn, it heats up [13]. To avoid heating that can cause a mechanical breakdown of the module, by-pass diodes are used. They allow the current to flow around the cells that are shaded. However, in such a case, the diodes distort the power characteristic of the module and multiple local maximum power points occur [14], but overall there is still one global MPP. While this is a very important

phenomenon that complicates MPPT, it is not considered in this thesis since the main objective is to investigate the effects of temporal irradiance changes and not spatial variations.

2.2 Maximum power point tracking

As discussed in the previous section, tracking the MPP requires continuous control of the operating voltage of the module output/converter input side of the system. A generic example of such a system is shown in Figure 2.4. Between the PV module and load, a converter is placed so that the voltage could be controlled. The DC-DC converter is governed by the MPP tracker which in nature is a computational component. The decision-making process of MPP tracker is based on logical principles combined into an algorithm. As an input for the algorithm, the MPP tracker receives measurements of the system depending on the requirements of the algorithm implemented. This could include measurements of input and output voltage and current, ambient temperature and irradiance.

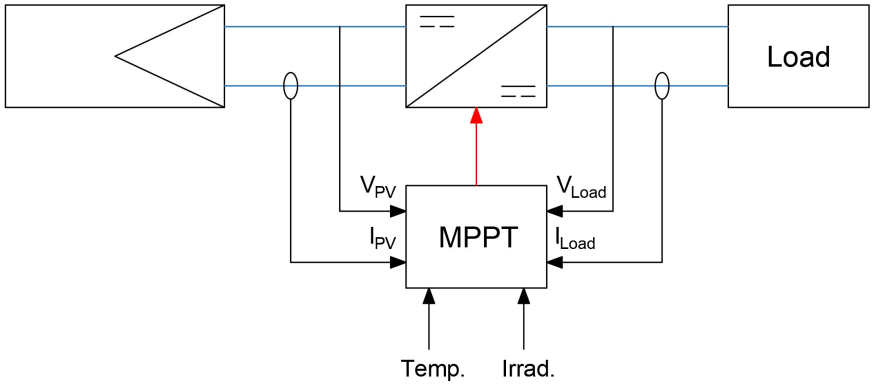

Figure 2.4: Generic maximum power point tracking system (adapted from [7])

A DC-DC converter is the component of MPP tracking system that physically changes operating voltage in the system, utilising one (or a few) switch(es) within its circuit [15]. A basic DC-DC converter schematic is shown in Figure 2.5a. Input voltage (V_d) is converted into an output voltage (v_o) by switching the switch periodically. The average output voltage V_o depends on the time fraction that the switch is on (t_{on}) and off (t_{off}) as seen in Figure 2.5b. Therefore, the control algorithm depending on predefined conditions decides the fraction of time within one period that the switch is on. The ratio of duration when the switch is on to the switching period T_s is called switch duty ratio D. It can be observed that for a period of time the circuit opens, resulting in loss of power, even if it is for a short period of time. This together with the physical properties (resistance, transient behaviour etc.) results in efficiency loss in the converter. However, the efficiency of maximum power point tracking as a whole depends on the way the switching is controlled or, in other words, on the accuracy of the algorithm implemented.

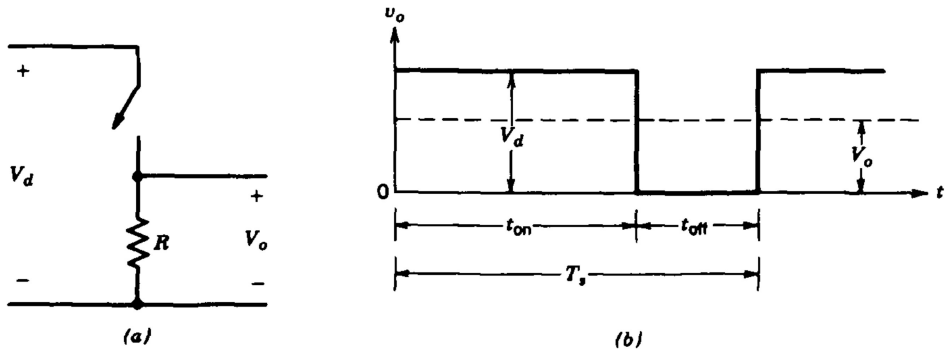

Figure 2.5: (a) DC-DC converter and (b) switch-mode DC-DC conversion (adapted from [15])

To date, at least 40 different algorithms for the purpose of MPPT have been proposed. They vary in terms of efficiency, complexity, speed, hardware and sensors required, cost etc. [9]. The algorithms can be classified into 5 groups [7]:

- Tracking with constant parameters. Such algorithms estimate MPP using predefined voltage values or a product of fixed coefficients and a single measurement from the system such as temperature, voltage or current. For example, the constant voltage (CV) method regulates the operating point to be close to a characteristic MPP voltage of the module (i.e. a datasheet value). In such a way it is assumed that the MPP stays the same at all times, disregarding the influence of irradiance and temperature, which results in poor performance of MPPT.

- Tracking with measurement and comparison. These techniques rely on two measurements (irradiance and temperature or current and voltage) to determine a pre-defined MPP. The look-up table method belongs to the measurement and comparison group. It compares irradiance and temperature measurements to a set of pre-saved values and selects a corresponding MPP voltage to be attained. The look-up table should include all possible scenarios of module operating conditions and therefore requires a lot of memory capacity.

- Tracking with trial and error. Trial in these algorithms means an attempt to reach MPP and error refers to the observation of change in OP as the result of an attempt. Then, depending on the found result, algorithms determine if OP is getting closer to MPP and decides on a new attempt. For example, if perturb and observe (P&O) algorithm perturbs voltage by a defined amplitude positively and a positive change in output power is observed, P&O judges that the direction was correct and the next perturbation will be positive as well.

- Tracking with mathematical calculations. Such methods rely on mathematical equations to estimate the MPP using measurements provided by sensors. One of the most popular algorithms in this category is the incremental conductance (IC) method. It is based on the fact that the slope of PV power characteristic at MPP is equal to zero, positive when voltage is lower than the one at MPP and negative when voltage is higher [9]. From these conditions, equations are derived and the algorithm solves them to determine the position of instantaneous OP on the P-V curve and decide on a required change accordingly.

- Tracking with intelligent prediction. These methods are the most complex as they employ data-driven or artificial intelligence techniques such as fuzzy logic or neural networks. Such intelligent tracking shows good performance in both steady-state and varying conditions. However, implementation of these methods can be costly not only because of required computational power, but also human resources. Performance of fuzzy logic control depends on the knowledge of the user or engineer that sets-up the controller, and neural network techniques requires periodic retraining and must be adapted for each installation separately.

All algorithms proposed have their own advantages and drawbacks. Usually, the selection of the algorithm depends on the system application, however, accuracy versus the cost of implementation plays the largest role. The best balance is achieved using P&O and IC algorithms, hence their popularity in research and industry [16]. These two methods have very similar efficiencies when IC algorithm is compared to optimised P&O, however, IC requires a complex control circuit. This leaves P&O algorithm to be most widely implemented in PV systems. Nevertheless, even with such widespread implementation, there are still some unknowns when it comes to its operation.

2.3 P&O algorithm

Perturb and Observe (P&O) algorithm is an MPPT technique that follows the logic of hill climbing. It attempts to reach the MPP in steps while observing if the power increases (the OP 'climbs up the hill' of P-V curve) or decreases (OP 'climbs down the hill' of P-V curve). While in literature there is a distinction made between P&O and hill-climbing methods, it is essentially the same concept [9]. Hill-climbing methods refer to step changes of the duty ratio of the converter and P&O to voltage. However, these two measures are closely interconnected as was seen in Figure 2.5 where it was shown how duty ratio

determines the average output voltage. Also, looking from another perspective, the necessary change in voltage is achieved by changing the duty cycle of the converter.

P&O requires current and voltage measurements from which power is computed. Based on values of the measurements from two time instances the control decision is made for a third one. The general rationale of the algorithm is to observe if the change in voltage made during the previous perturbation results in an increase or decrease in power [16] [17]. If an increase is observed, the next perturbation would be in the same direction as previous and if a decrease was detected next perturbation would be in the opposite direction. Here, the direction refers to the sign of perturbation. Perturbation amplitude ΔV is one of the two parameters of P&O. The algorithm flowchart is provided in Figure 2.6. The first condition the algorithm evaluates is if operating power at the current instance is equal to previous power (P(t)=P(t-1)). If a positive conclusion is made no change is implemented in operating voltage, if the answer is negative another conditional statement is checked to determine which way the previous perturbation was directed and what is the outcome of it. To evaluate the outcome, the current operating power is compared to one at the previous instance by solving inequality P(t)>P(t-1). If the inequality is true and the previous perturbation was negative (V(t)<V(t-1)) next perturbation will be positive (V(t+1)=V+ΔV) which means that the perturbation direction will be changed, but if V(t)⩽V(t-1) perturbation will be kept negative (V(t+1)=V-ΔV). If P(t)>P(t-1) is not true the algorithm will inspect if V(t)>V(t-1). If this statement is fulfilled, the next perturbation will be positive, if not - negative. The summary of the decision-making process of the P&O algorithm is provided in Table 2.1 [9]. This process is continuously performed at each perturbation. Frequency of the perturbations is determined by the second P&O parameter - sampling interval T_a. Performance of the algorithm depends on both of the P&O parameters as well as the ambient conditions of irradiance and temperature. Such conditions can be identified as either steady-state or dynamic.

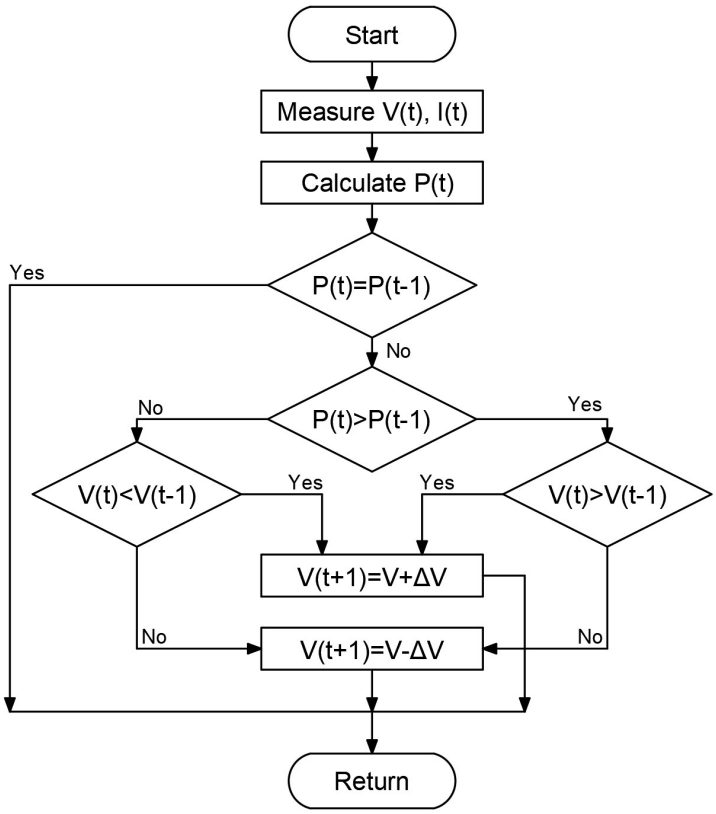

Figure 2.6: P&O algorithm flowchart (adapted from [17])

Because of the continuous perturbations voltage (and in result power) is constantly adjusted which induces oscillations around the MPP, and this is a consequence of available power loss [16]. The oscillations are presented in Figure 2.7. If irradiance and temperature are constant the P-V curve is

Table 2.1: Summary of P&O algorithm

Previous perturbation	Power change	Next perturbation
Positive	Positive	Positive
Positive	Negative	Negative
Negative	Positive	Negative
Negative	Negative	Positive

constant as well and P&O is operating in steady-state conditions. In such case, once the a point close to MPP (point 2) is reached algorithm still makes perturbations to the right and left of the MPP as shown in 2.7a because of the decision process presented in Table 2.1. This is one of the main drawbacks of the P&O algorithm. The voltage signal in time is shown in 2.7b where the operating points are given in red. The voltage difference between the OPs is equal to perturbation amplitude ΔV and the number of oscillations is determined by the sampling period T_a. While both parameters are very important, in a steady-state scenario a change of T_a would not have a major effect in terms of power loss - the total amount of time that the OP is not equal to MPP would be the same, only the number of changes in OP within a period of time would differ. On the other hand, ΔV influences the power loss highly: the larger the ΔV the larger the oscillations in the amplitude of voltage (and power) and the more power output of the PV module not utilised. To that end, it would be beneficial to reduce ΔV to a minimum and suppress the fluctuations. However, such an approach would decrease the overall performance of P&O since in most locations irradiance is rarely stable and hence steady-state scenario is not the case at all times.

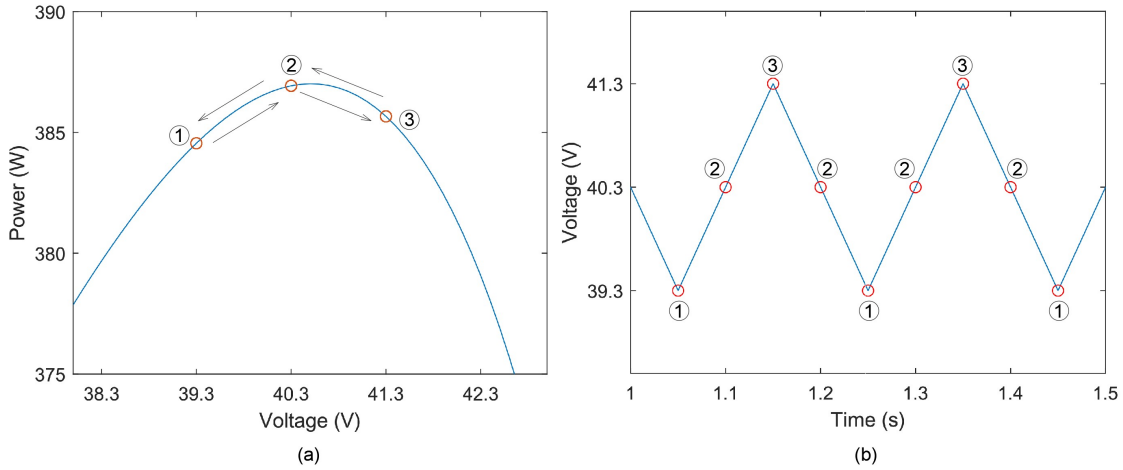

Figure 2.7: Steady-state operation of P&O algorithm on P-V curve and in time series ($T_a = 0.5s$ and $\Delta V = 1V$)

During dynamic conditions of the P&O operation, irradiance can change rapidly. Since the module output is highly dependant on irradiance incident on the module, change in irradiance results in a change in the module output in terms of P-V curve (as was discussed in Section 2.1). If such change is gradual enough algorithm performance would not deteriorate majorly as shown in Figure 2.8a, where the MPP points on all intermediate P-V curves are indicated by $*$. In such a case, OP values do not diverge from MPP much and power loss can be comparable to one in steady-state conditions. However, if irradiance change is rapid, P&O algorithm fails since the OP moves away from MPP instead of closer [8] [16] (Figure 2.8b). Such confusion happens because the algorithm is not able to distinguish whether a change in power output happens due to the perturbation or because of the irradiance change [8]. The reason behind the failure of P&O under rapidly changing conditions of the algorithm is presented in Figure 2.9. Figure 2.9a shows a case when at k^{th} perturbation the OP is at MPP. Then a positive perturbation is executed to point A and the resulting difference in power is indicated by ΔP_d. If in the meantime P-V curve shifts up the OP ends up in point B instead of A and a positive change due to a change in irradiance ΔP_s will happen. However, since the overall power change is still negative, the next perturbation will be negative (as per Table 2.1) and the OP will move closer to MPP as would be expected. However, such behaviour is obtained only when ΔP_d is larger than ΔP_s. Figure 2.9b presents

the contrary, where the increase in power due to irradiance change is larger than the decrease as a consequence of the perturbation. In cases like this, a positive perturbation results in a positive increase in power and hence the direction of the next perturbations would not be changed, which leads the OP away from the MPP. If the rate of the irradiance increase does not reduce such divergence would continue further and further away from the MPP and a substantial amount of available power would be lost.

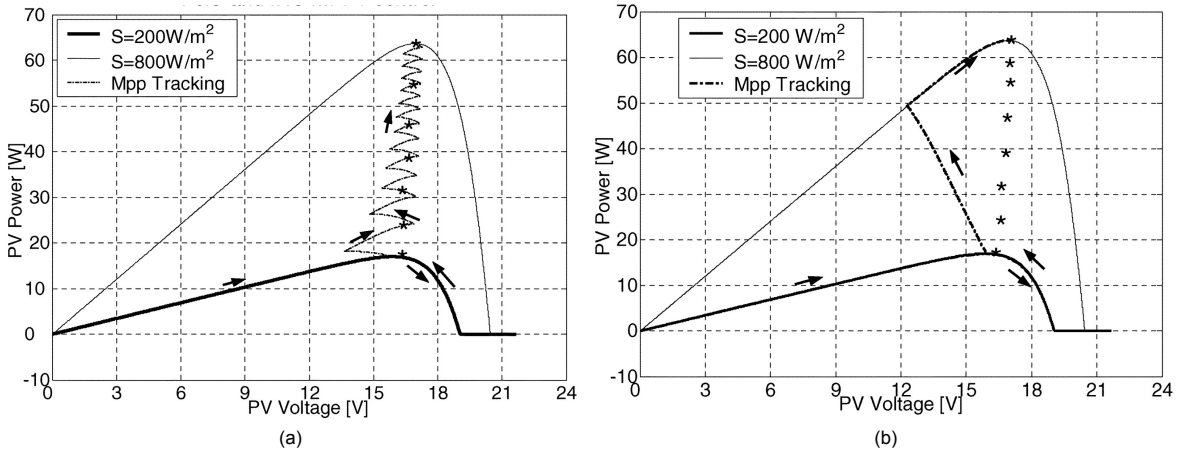

Figure 2.8: Operating point changes as governed by P&O algorithm in (a) slowly and (b) rapidly changing conditions [8]

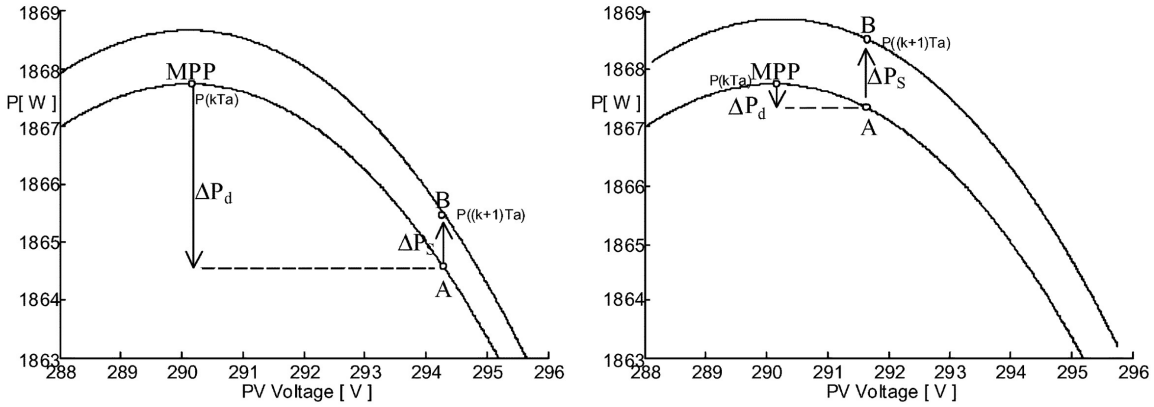

Figure 2.9: P&O operation in dynamic conditions when parameters are selected (a) properly and (b) improperly [8]

To prevent P&O algorithm confusion and loss of power, parameters should be optimised. Femia et al. [8] argued that optimisation is usually done by trial and error and, to that end, proposed a methodology to obtain proper sampling interval and perturbation amplitude based on theoretical analysis. Firstly, it is determined that the sampling period should be as low as possible for the P&O to capture even the smallest changes that are happening due to irradiance variation. However, a minimum limit should be established because of the transient behaviour of the switch device that is the DC-DC converter. If the sampling period is too small the P&O could make mistakes due to the PV systems' transient oscillations [8] [18]. This minimum limit depends on the inductance and capacitance of the PV side of the system and resistance of MPP. The latter relies on the output P-V curve of the PV module and, in turn, on the irradiance. For determining a minimum value of the perturbation amplitude, the inequality discussed previously $|\Delta P_d|>|\Delta P_s|$ (refer to Figure 2.9) is solved. The solution shows that minimum perturbation amplitude depends on voltage and resistance at MPP (which as mentioned depends on irradiance) as well as the rate of change of irradiance within the sampling interval. This estimation provides a minimum perturbation amplitude so that the algorithm does not get confused if the irradiance rate of change used in the calculation is not exceeded. However, the authors do not propose how to exactly estimate the irradiance used for determining MPP and the irradiance rate of change so that the optimisation of

parameters would be valid in real-world conditions. This together with the required knowledge about the topology of the converter makes parameter estimation difficult. To provide an understanding of magnitudes of these parameters, Table 2.2 summarises values found in literature.

Table 2.2: P&O algorithm parameters reported in literature

Reference	T_a	ΔV or ΔD
[6]	50 ms	ΔD = 0.01
[8]	20, 10, 3.3 ms	ΔD = 0.005, 0.001, 0.1
[16]	-	ΔV = 2 V (0.37 %$V_{(oc)}$)
[18]	10 - 50 ms	ΔV = 0.586 %
[19]	0.1 ms	-
[20]	1 s	ΔD = 0.5 - 3 %
[21]	0.1 ms	ΔD = 2 %

2.4 MPPT algorithm efficiency

To evaluate performance and effectiveness of an algorithm under steady and rapidly changing conditions, algorithm efficiency is introduced. Instantaneous efficiency can be calculated as the ratio of obtained power at the OP and available maximum power at MPP. However, usually, energy efficiency is used where power values are integrated for a defined period of time (T_M) as given in Equation 2.1 [6]. However, since the average value of a function (f) is defined as given in Equation 2.2, it is adequate to use average OP and MPP power values.

$$\eta_{MPPT} = \frac{\int_0^{T_M} V_{OP}(t) \times I_{OP}(t)dt}{\int_0^{T_M} P_{MPP}(t)dt} = \frac{\int_0^{T_M} P_{OP}(t)dt}{\int_0^{T_M} P_{MPP}(t)dt} \tag{2.1}$$

$$\bar{f} = \frac{1}{b-a}\int_a^b f(x)dx \tag{2.2}$$

Efficiency of the P&O algorithm has mostly been studied to compare it to other algorithms. Usually, to perform such comparisons, an experimental set-up is employed that includes a PV array simulator and DC-DC converter with a microcontroller [6] [18] [19] [21] [22]. Alternatively, efficiency is obtained by mathematical modelling of each component [16]. However, all comparative studies rely on predefined irradiance change events. For example, Hohm and Ropp [18] used a relatively random sequence lasting for over 9 min, which was aimed to represent a partially cloudy day. de Brito et al. [19], Pandey et al. [21] and Jeddi and Ouni [22] defined step changes for very short time periods up to 1 s, while Faranda and Leva [16] studied efficiency of algorithms in 14 irradiance change events lasting for 0.5 s. It is worth mentioning, that step variations of irradiance do not occur in real-world scenarios as in nature two values of the same measurement at the same time are not possible, however, they provide insight into the response time of the algorithms.

To regiment studies of inverter performance, a standard test procedure (prEN 50530) has been developed [23] and this test was implemented to study efficiency of P&O and IC algorithms by Ishaque et al. [6]. The test includes continuous and increasing ramping up and down at two irradiance levels for a total of 5 hours as shown in Figure 2.10. The study found that on average P&O efficiency is higher when irradiance level is higher as shown in Figure 2.11a which is argued by the authors to be the result converter characteristics. Low efficiency values are also seen in Figure 2.11b at low power (and irradiance) and are explained to exist due to the low PV output current present in such conditions which means that even with small perturbation amplitude the variation in current is significant.

There were two research papers found that utilized real irradiance data in their studies of efficiency. Firstly, Yan et al. [20] used the classification of irradiance conditions to perform optimisation of the P&O parameters by obtaining and comparing yield in each case. To do so, 1 min resolution irradiance data was used to simulate PV power output and obtain yield values experimentally. In the second

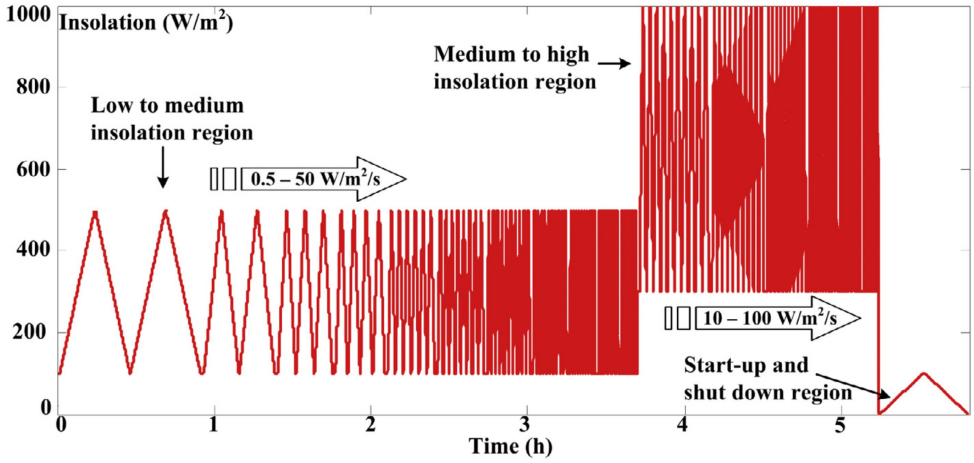

Figure 2.10: prEN 50530 standard dynamic test profile [6]

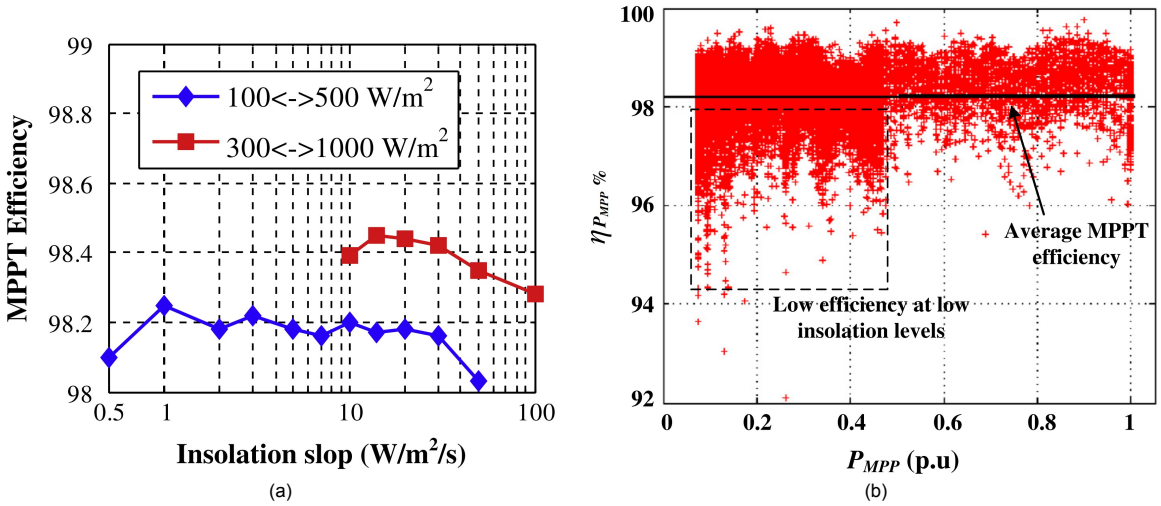

Figure 2.11: (a) Average P&O efficiency against insulation slope (ramp rate) and (b) instantaneous P&O efficiency for the whole profile [6]

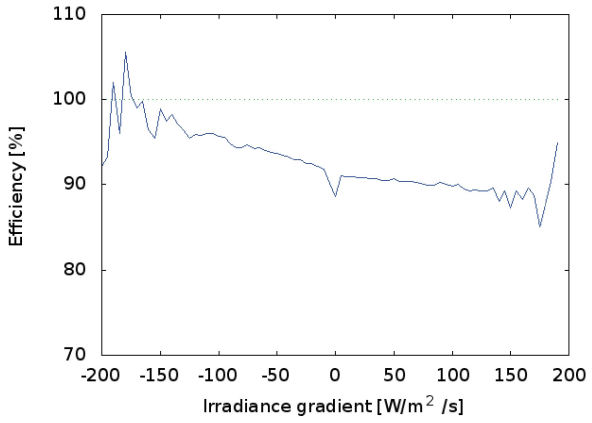

Figure 2.12: Averaged inverter efficiency for different irradiance gradient (i.e. ramp rate) values [24]

study, Piotrowicz and Marańda [24] examined the performance of MPPT in a field-installed inverter fed by 1 kWp capacity PV installation in Łódź, Poland. The data analysed comprised DC, AC power and irradiance values sampled every 5 s for a year. While the study does not specify what kind of algorithm

is implemented in the inverter, it is understandable since inverter manufacturers usually do not provide such information in their datasheets or manuals. Also, the efficiency was calculated using the input and output power of the inverter which implies that the efficiency includes not only MPPT but also the DC to AC conversion efficiency. Results of this study included Figure 2.12 which similarly to Figure 2.11a shows lower efficiency at the higher slope (i.e. ramp rate). However, in this case, both positive and negative values are considered and it noted that efficiency is higher during negative ramping. This is explained by the fact that the inverter components store energy which is released when irradiance drops. In summary, as per reviewed literature, MPPT efficiency is lower during large ramping events and at lower irradiance levels.

2.5 Irradiance variability

Irradiance variability refers to the changes that happen in the irradiance profile throughout a year, a day or even a minute. The temporal scale on which variability is studied depends on the specific research goals, however, the most common motivation is to examine irradiance variability so that the PV power output variance could be determined. This is necessary because with increasing renewable energy production grid stability becomes an issue since the most prominent renewable sources - wind and solar - are dependant on the weather conditions which vary greatly. While fluctuations of PV power injected into the grid are present on both large (e.g. yearly) and on very small (e.g. sub-minute) scales, they are mostly studied on a minutely resolution. Two of the reasons for this are the smoothing or averaging effect of decreasing temporal resolution and the available irradiance data sources. The averaging effect is illustrated in Figure 2.13 [11]. It can be observed that if irradiance is sampled at 1 min quite a lot of variation in irradiance is retained. However, averaging for 5 min reduces the abrupt changes and for 10 min - even more. Averaging for even higher periods removes most of the original variation and at 120 min only a few data points are left. Due to the utilization of satellite imagery, most of the databases for irradiance provide only hourly averages of irradiance, but as seen in this figure such data would not be very beneficial in studying variability. On the other hand, even the 1 min data are averaged values of higher resolution, however very high resolution data are difficult to attain for a specific location because of the measurement procedures as well as data storage.

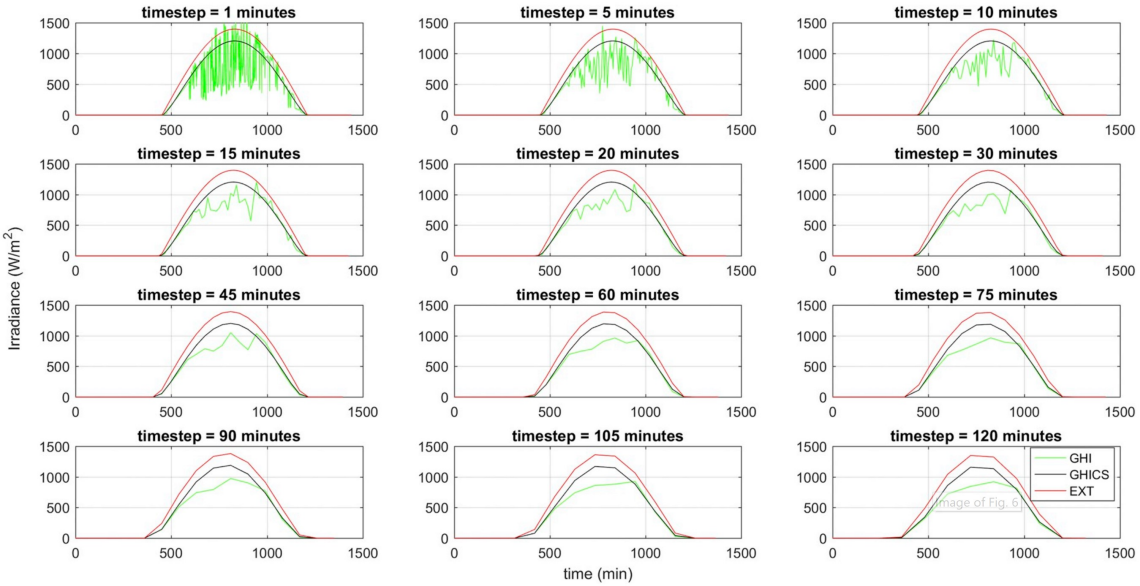

Figure 2.13: Temporal resolution averaging effect on irradiance time-series (GHICS - clear sky irradiance and EXT - extraterrestrial irradiance) [11]

Low temporal resolution data are quite easily accessible through use of databases such as Meteonorm [25] or PVGIS [26]. Such databases usually provide hourly irradiance data obtained from ground-based measurements or satellite-derived data. One major advantage of hourly databases is

that irradiance data could acquired for almost any location [27]. Also, use of hourly data allows storage of data describing long time spans like multiple years. However, the smoothing effect of aggregating irradiance data for as long as an hour reduces variability in the data immensely as was discussed before. This means that studying variability using such data is pointless. On the other hand, minutely data can be obtained by ground-based measurements only, which makes long-term and high-quality datasets costly and reduces the number of locations where minutely data are available [28]. For example, the largest network of irradiance measurement stations that acquire 1 min irradiance (and other meteorological) data is the Baseline Surface Radiation Network [29] that includes 74 stations around the globe which does not make for extensive coverage. To that end, research has focused on downscaling data from hourly values to minutely synthetically. This is done by extracting statistical features form the low resolution data and applying them to the 'gaps' between datapoints in original dataset [28]. However, the accuracy of such models depends on the resolution of the data that is being downsampled and the resolution it is being downscaled into, or in other words how many data points are being created artificially. Thus sub-minutely data most likely could only be produced from data sampled in the range of minutes. Acquiring real measured sub-minute irradiance data for a specific location is difficult. If such data are necessary, one needs to install a radiometer themselves which makes data expensive and lenghty to obtain.

When it comes to researching variability, most of the literature is concerned with how to quantify it and such quantities are then computed for specific locations to provide a better irradiance resource analysis. Also, comparisons between the metrics are often performed. Castillejo-Cuberos and Escobar [11] have provided an overview of the proposed metrics in literature as well as a classification of them. The classes are as follows:

- Statistical metrics rely on concepts from the field of statistics. Usually, metrics like standard deviation or mean values within a certain period are utilized. The values themselves can vary, but usually, clear-sky and/or clearness indexes or increments of them are used. Both of these indexes describe how much irradiance is retained during cloud shading conditions, however, the clearness index does not assume any absorption of irradiance in the atmosphere. Other than the standard statistical measures, metrics such as total harmonic distortion or coefficient of variation can also be classified as statistical. The prior is obtained by performing Fourier transform on the irradiance dataset and the latter is the ratio between the standard deviation and mean value of irradiance change amplitude.

- Meaning of deterministic approaches stem from a physical interpretation of variability. One of the more popular variability metrics, in general, is variability index VI as proposed by Stein et al. [30]. It is computed as shown in Equation 2.3:

$$VI = \frac{\sum_{k=2}^{n} \sqrt{\left(GHI_k - GHI_{k-1}\right)^2 + \Delta t^2}}{\sum_{k=2}^{n} \sqrt{\left(CSI_k - CSI_{k-1}\right)^2 + \Delta t^2}} \tag{2.3}$$

  where GHI is the global horizontal irradiance, CSI is clear-sky irradiance and Δt is data resolution with which the calculation is performed. It physically means the ratio of the length of irradiance versus time curve and length of clear-sky irradiance time-series curve. Also, it is important to note that VI depends on the resolution of the data since larger GHI changes will be observed at a smaller scale, while there would be barely any difference in what resolution the clear-sky irradiance is computed.

- Probabilistic quantifiers aim to describe the data distribution through a cumulative distribution function (CDF). One such metric is the variability score VS_{cdf} and it can be visualised as the shortest distance between the CDF curve of absolute irradiance changes and the point (0,1). For example, if variability is negligible the CDF curve will peak at a point close to (0,1) and the distance, and in turn VS_{cdf}, will be small indicating small variability; the opposite would be the case if highly variable irradiance changes would be cumulatively distributed.

2.6 Summary

In this chapter, the non-linear output I-V and P-V curves of the PV module were discussed and MPP was introduced as the operating point at which maximum power would be attainable from the PV module at any instance. However, it changes constantly because of the change of ambient conditions - irradiance and temperature - as PV electrical output is dependant on them. Because of the change in P-V curves, the MPP changes as well. This indicates a need for tracking the MPP continuously. MPPT is done by use of a DC-DC converter which is able to change the operating point by switching the circuitry on and off. The regulation of voltage to reach MPP is governed by a MPPT algorithm.

While there are many algorithms proposed, P&O algorithm is mostly implemented in the industry and receives the most attention from the research community. The P&O algorithm, as the name suggests, changes operating voltage in predefined step size of the perturbation amplitude ΔV, observes whether it results in a positive or negative change in power and changes the direction of the next perturbation accordingly. Even though the P&O algorithm is popular, it also has its drawbacks. In a steady-state scenario when MPP is reached the OP oscillates around it and the magnitude of oscillations is determined by ΔV, hence it would be beneficial to keep it low. However, under dynamic conditions P&O with low ΔV could get confused in which direction to perturb the voltage and performance would be poor. Nevertheless, with proper optimisation of ΔV as well as sampling period T_a an adequate operation can be achieved.

Performance of P&O and other algorithms is evaluated through efficiency calculations which is the ratio of operating power and maximum power available. There are a number of studies done, mainly for purpose of comparison, on P&O algorithm efficiency. However, for calculations or experimental simulations, most of them assume predefined irradiance changes lasting a very short period of time. The few found studies using real irradiance data were judged inconclusive or limited in results as fluctuations in irradiance are only described in ramp rates. To that end, this thesis will aim to fill a gap of using high-frequency irradiance data so that the maximum of the variations of irradiance could be retained and will aim to relate irradiance variability to P&O efficiency. To describe the relationship of P&O efficiency and variability, variability needs to be quantified. For this many metrics has been proposed in the literature, indicating that there is no common consensus of how variability can be best evaluated. To that end, one of the most popular metrics - variability index - will be used as well as other conventionally utilized statistical features.

3

Methodology

To answer the research questions raised in Chapter 1 a methodology was formulated and is presented in this chapter. The framework is showcased in Figure 3.1. Firstly, a dataset of P&O efficiency values and variability metrics must be created so they can be analysed against each other. To calculate variability metrics specific parameters describing solar irradiance are necessary. For this purpose time-stamped irradiance data containing GHI, DHI and DNI values is acquired. For each timestamp of this dataset Sun's position in the sky is determined by calculating its elevation and azimuth. These features are then used to estimate extraterrestrial - incident on Earth's atmosphere - irradiance and clear-sky irradiance that would be measured when no clouds or other shading objects are present. Using all these acquired and calculated irradiance features, variability within a period of time can be quantified through variability metrics.

Determining P&O efficiency requires power at MPP (P_{MPP}) and operating or P&O power ($P_{P\&O}$) values. To obtain them, PV module output is modelled using irradiance incident on the module and PV module parameters. Incident irradiance is calculated using a geometrical model utilizing acquired irradiance and calculated Sun's position data. The PV model provides maximum power point values and I-V curves. The latter is used to determine the operating point through the implemented P&O algorithm. To do so, P&O parameters - sampling interval and perturbation step - are set. Finally, the resulting P&O power output is used to compute P&O efficiency by dividing with previously acquired maximum power.

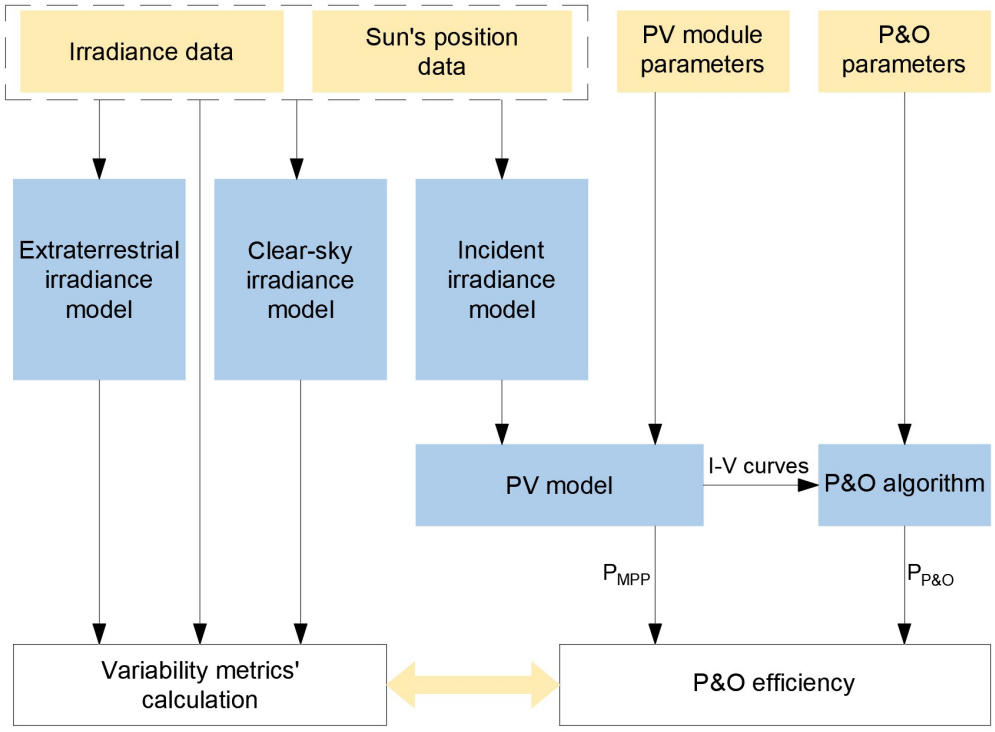

Figure 3.1: Framework for P&O efficiency and variability metrics' calculation

To elucidate each step of the mentioned calculations, this chapter is structured as follows. Irradiance and Sun's position data are discussed in Section 3.1. Models used to determine clear-sky and extraterrestrial irradiance are described in Sections 3.2 and 3.3 respectively. Furthermore, the incident irradiance model is explained in Section 3.4. Section 3.5 details the process of PV module output calculations using a PV model. Implementation of the P&O algorithm to determine the operating or P&O power are discussed in Section 3.6. Lastly, variability metrics' calculations are described in Section 3.7.

3.1 Irradiance and sun's position data

Irradiance data used in this research was obtained from an openly available National Renewable Energy Laboratory database [31]. The dataset contains GHI, DHI (diffuse horizontal irradiance) and DNI (direct normal irradiance) values sampled every 3 seconds from March 16, 2010 to October 31, 2011. However, for the sake of consistency of the results only one full year from March 16, 2010 to March 15, 2011 is considered for this research. This data was collected using a rotating shadowband radiometer (RSR) - a measurement instrument that uses a silicon-based photodiode pyranometer to measure the global and diffuse solar irradiance. This device is part of the Oahu solar measurement grid and is located in the southwestern part of the Oahu island, Hawaii as shown in Figure 3.2. This location and can be described as having an equatorial savanna with dry winter (Aw) Köppen-Geiger climate type [32]. Typical daily irradiance profiles as measured by RSR in Oahu are shown in Figure 3.3. Hawaii is located around 2300 km north of the equator and does not experience major seasonality and large differences in maximum irradiance values throughout the year. However, with climate type falling under the tropical category, variability of irradiance is persistent due to moving scattered clouds, the sky is rarely fully clear in this location.

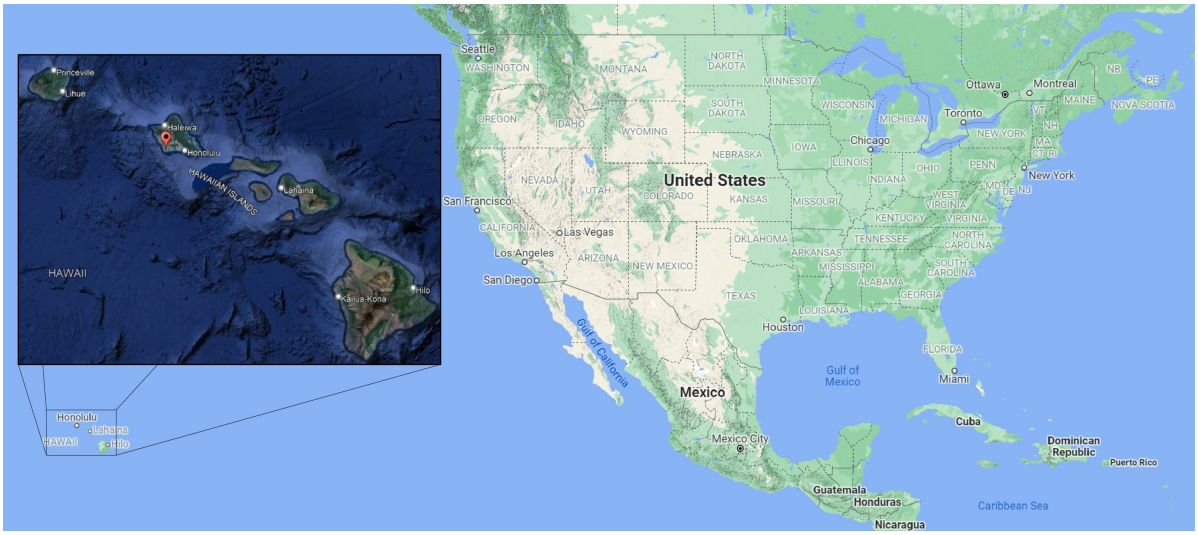

Figure 3.2: RSR location in Oahu, Hawaii (red pointer icon)

The original dataset with irradiance values is expanded to include parameters describing Sun's position - azimuth and elevation angles. These angles are used to describe Sun's position in a celestial sphere which has an arbitrary radius and is concentric to the observer [13]. Position of the Sun is defined using a horizontal coordinate system, as shown in Figure 3.4, where solar elevation angle is denoted as θ_{El} and azimuth - as θ_{Az}. Zenith angle is also often used in irradiance calculations, it is denoted by θ_Z and is equal to $90° - \theta_{El}$. The position of the Sun depends on the observer location on the Earth, time of the year and of the day and hence angles describing it are derived from time. For each timestamp of the acquired irradiance dataset angles are calculated using the Equations 3.1 - 3.7 [33].

$$\cos\theta_Z = \cos\phi\cos\delta\cos\omega + \sin\phi\sin\delta \tag{3.1}$$

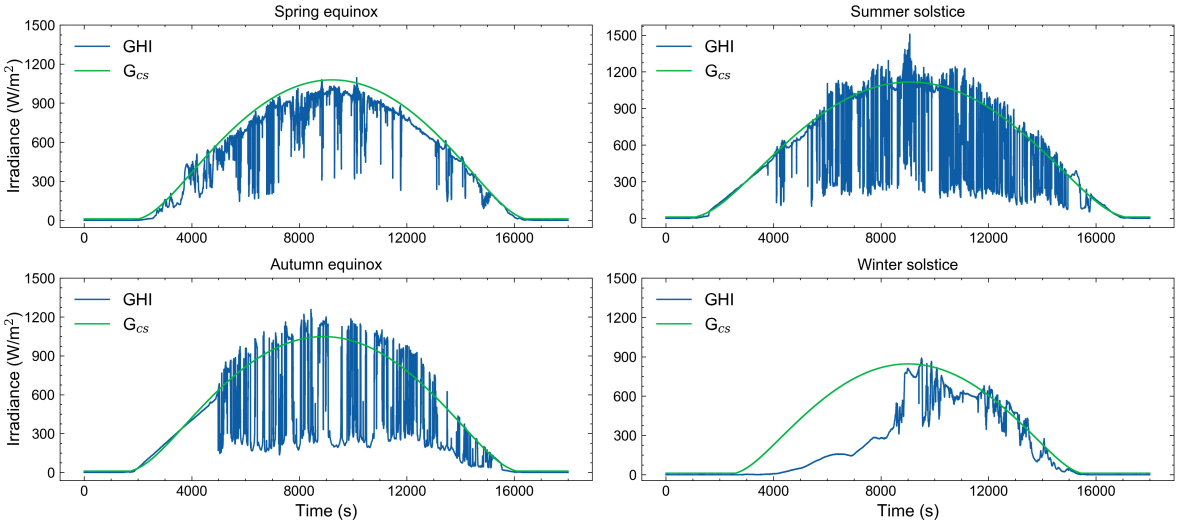

Figure 3.3: Monthly and yearly average P&O efficiency

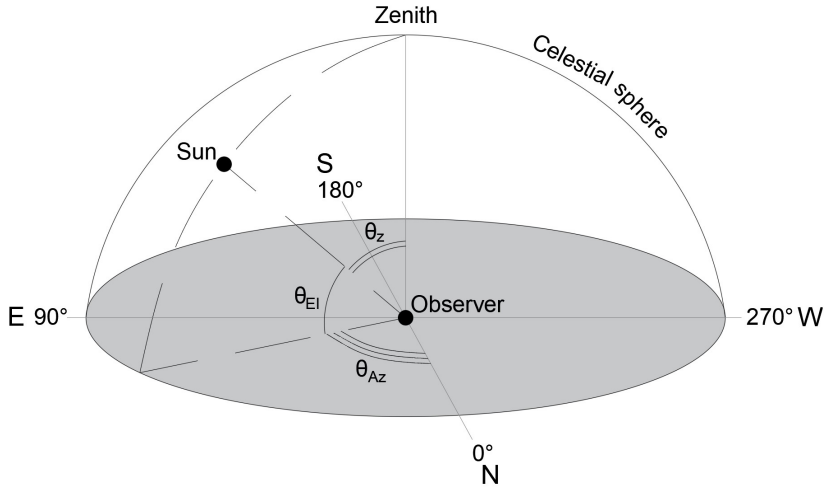

Figure 3.4: Solar position in a horizontal coordinate system (adapted from [13])

where ϕ is the latitude of the observer, δ is the solar declination angle and ω is hour angle. Solar declination angle is the angle between the line joining centers of Sun and Earth and Earth's equator plane equal to ~+23.5° at summer solstice and ~-23.5°at winter solstice in the northern hemisphere. The hour angle ω is an angle between two planes: one contains Earth's axis (celestial pole) and the center of the Sun and the other is the meridian plane which includes Earth's axis and zenith [34]; it changes by 15° every hour. The solar declination angle is calculated using Equation 3.2:

$$\delta = 23.45^\circ \sin\left(360^\circ \frac{284 + n}{365}\right) \tag{3.2}$$

where n is the day of year (DOY) - number between 1 and 365. Hour angle is computed as follows (Equations 3.3 - 3.6):

$$\omega = (t_s - 12) * 15 \tag{3.3}$$

$$t_s = H + (\lambda/15) - TZ + t_{ad} \tag{3.4}$$

where H is minutes in hours $(hour + (minutes/60))$, λ is longitude of the observer, TZ is time zone east from Greenwich mean time and t_{ad} is civil time adjusted to solar time. The latter is calculated using Equation 3.5:

$$t_{ad} = 3.82[0.000075 + 0.001868\cos B - 0.032077\sin B - 0.014615\cos(2B) - 0.04089 * \sin(2B)] \tag{3.5}$$

where B is:

$$B = 360^{\circ}\left(\frac{n-1}{365}\right). \tag{3.6}$$

Azimuth of the sun is computed using Equation 3.7 [35], it was implemented using PVLIB toolbox in Matlab [36].

$$\theta_{Az} = \arctan 2\left(\frac{\sin\omega}{\cos\omega\sin\phi - \tan\delta\cos\phi}\right) \tag{3.7}$$

3.2 Clear-sky irradiance model and k_c

Clear-sky irradiance represents irradiance values that would be observed in a specific location if the sky was clear. It is important to obtain these values since comparing them to real measurements of irradiance provides a lot of insight into the conditions of irradiance in terms of how much irradiance is lost due to obstructions like clouds or other shading objects. To determine this, a clear-sky index is used. It is defined as the ratio of measured irradiance and clear-sky irradiance (Equation 3.8 [10]). It can be calculated using global horizontal irradiance or its direct and diffuse components. When looked at yearly or daily scales, it also removes variance of irradiance values due to Earth's movement around the Sun and its own axis [37].

$$k_{c(GHI)} = \frac{GHI_{measured}}{GHI_{clear-sky}} = \frac{GHI}{G_{cs}} \tag{3.8}$$

In this research, to obtain clear-sky irradiance ESRA (European Solar Radiation Atlas) model was implemented. While there are many other clear-sky irradiance models proposed in the literature, ESRA model is one of the best performing models albeit it being simple and robust [38]. The goal of any clear-sky irradiance model is to estimate how much of the incoming irradiance is dissipated due to interaction with particles in the Earth's atmosphere. ESRA model takes into consideration this attenuation by use of Linke turbidity factor. It is a convenient approximation of the irradiance absorption by water vapour and both absorption and scattering by aerosol particles in reference to a clean and dry atmosphere [39]. In this study, monthly Linke turbidity factor values for Oahu, Hawaii (for air mass equal to 2) were obtained from the Meteonorm 8 database [25] and assumed to not change throughout the days of the month. The proceduce of ESRA model as implemented in this thesis is given in Appendix A.

3.3 Extraterrestrial irradiance model

While clear-sky irradiance provides an understanding of what irradiance would reach Earth's surface under clear skies, there are uncertainties associated with its values because light absorption and scattering in the atmosphere has a complex physical mechanism and it varies in time more than a model can capture [10]. To avoid such uncertainty the extraterrestrial irradiance could be used instead of clear-sky. Extraterrestrial irradiance obtains values of irradiance that is incident on the Earth's atmosphere and hence avoids assuming any processes when light traverses through it. To examine irradiance conditions, extraterrestrial irradiance can be used similarly to clear-sky irradiance - by calculating a clearness index k_t (Equation 3.9 [10]). Same as the clear-sky index, it removes the variance of irradiance due to Earth's movement, however, the clearness index now gives a value of how much light intensity is lost due to not only the clouds but the traversion through the atmosphere as well, which is not always desirable.

$$k_{t(GHI)} = \frac{GHI_{measured}}{GHI_{extraterrestrial}} = \frac{GHI}{G_0} \tag{3.9}$$

This study uses extraterrestrial irradiance values obtained employing a method as used in HOMER (Hybrid Optimization of Multiple Energy Resources) software [40]. Firstly, extraterrestrial irradiance at a normal plane to the Sun's rays is calculated using Equation 3.10:

$$G_0' = I_0 \left(1 + 0.033 \cdot \cos \frac{360n}{365}\right) \tag{3.10}$$

where I_0 is the solar constant - normal extraterrestrial irradiance, equal to 1367 W/m^2. Then G_0' is projected to a horizontal plane and global horizontal extraterrestrial irradiance is obtained using Equation 3.11:

$$G_0 = G_0' \cos \theta_Z \tag{3.11}$$

3.4 Incident irradiance model and module temperature

The last irradiance model in this framework is used to calculate irradiance incident on the module's surface at each timestamp of the Oahu irradiance data. This irradiance consists of three components - direct, diffuse and reflected - as shown in Equation 3.12 [13]. The three irradiance components are adjusted to conform with on-site conditions such as module's position, horizon and ground coverage. Direct irradiance component is adjusted by use of angle of incidence (AOI) (Equation 3.13) calculated as given in Equation 3.14. Calculations of diffuse (Equation 3.15) and reflected (Equation 3.16) irradiance introduce a new term called sky view factor (SVF) which is the fraction of the sky that the module can receive diffuse irradiance from or, in other words, the fraction of the sky that is 'visible' to the module. SVF depends on the obstructions of the horizon by nearby objects and on the position of the module. The latter dependency is given in Equation 3.17. For the computation of reflected irradiance incident of the module albedo (α) is also required. It describes the reflectively of the surface that the module is placed on. In this framework albedo is taken as 0.2 - a value often considered when the surface is green grass.

$$G_{inc} = G_{dir} + G_{diff} + G_{ref} \tag{3.12}$$

$$G_{dir} = DNI * \cos AOI \tag{3.13}$$

$$AOI = \arccos\left(\cos \theta_{El}^M \cos \theta_{El} \cos\left(\theta_{Az}^M - \theta_{Az}\right) + \sin \theta_{El}^M \sin \theta_{El}\right) \tag{3.14}$$

where θ_{El}^M is elevation of the module equal to 90° - θ_M (θ_M is the tilt angle of the module) and θ_{Az}^M is the azimuth of the module (equal to 180° if facing due South).

$$G_{diff} = DHI * SVF \tag{3.15}$$

$$G_{ref} = GHI * \alpha * SVF \tag{3.16}$$

$$\text{SVF} = \frac{1 + \cos \theta_M}{2} \tag{3.17}$$

While in this study the module is considered to be placed horizontally (i.e. tilt is 0°) and in such case azimuth of the module does not have an impact, also the horizon is assumed to be completely clear, the previously mentioned calculations were implemented to the framework to make it more robust and applicable in other cases.

Module output is also dependant on its operating temperature. However, since this study is concerned with the variability of the irradiance only a simple Sandia temperature model [41] is used and is given in Equation 3.18:

$$T_m = G_{inc} * e^{a+b*WS} + T_a \tag{3.18}$$

where T_a is the ambient temperature, WS is the wind speed and a and b are parameters dependent on module construction and materials. In the case of this study, ambient temperature is considered to be constant 25°C, and wind speed - constant 3 m/s. The module structure is assumed to be glass/cell/glass and the module to be mounted on an open rack, in which case a = -3.47 and b = -0.0594.

3.5 PV output model

To implement the P&O MPPT algorithm, I-V curves at each step of perturbation are necessary. Since P&O algorithm is run at much smaller intervals than the 3 s intervals of sampled irradiance data, an assumption is made that irradiance values change linearly between each 3 s timestamp. Such assumption is necessary because 3 s values of irradiance are the average of values within the period and such averaging removes information about the variability of the irradiance. Even though there are methods to estimate the averaged values using downsampling techniques, they are usually implemented to downsample data to much lower temporal resolutions than the sampling period of P&O (i.e. from 1 hour or 30 min to 1 min) [42] [28]. There is a possibility that the same models could be used for downscaling to much higher temporal resolutions if a proper validation is performed, however, since such validations are not available in the literature, a much simpler approach is taken and irradiance values are linearly interpolated without assuming any variability within 3 s periods.

Other limiting assumptions made to obtain I-V curves at each sampling time of the P&O are: (a) PV module response to irradiance is faster than the sampling period of P&O; (b) response of the current and voltage measurements necessary for P&O algorithm are also instant; (c) irradiance on the module is uniform i.e. there is no partial shading. The last assumption is major in the sense that module I-V curves are much different when the module is shaded partially, which largely affect the performance of P&O. However, since the goal of this study is to investigate P&O efficiency relationship to irradiance variability, this assumption is deemed appropriate.

To obtain the module output in response to changing irradiance a single diode model of the PV module (as shown in Figure 3.5) is implemented using Equation 3.19 [43]:

$$I = I_{ph} - I_0 \left[\exp\left(\frac{V + R_s I}{n_s V_t a_{id}} \right) - 1 \right] - \frac{V + R_s I}{R_p} \tag{3.19}$$

where I_{ph} and I_0 are the PV and reverse saturation currents respectively. V_t is thermal voltage as given in Equation 3.20. R_s is the series resistance of the module and R_p is parallel or shunt resistance. a_{id} is the diode ideality constant $(1 \leqslant a_{id} \leqslant 1.5)$ and n_s is the number of cells connected in series to form the module. However, in practical PV modules R_s is low and R_p - high and hence they can be neglected and module output current calculated as given in Equation 3.21.

$$V_t = \frac{kT_m}{q} \tag{3.20}$$

$$I = I_{ph} - I_0 \left(\exp\left(\frac{V}{n_s V_t a_{id}} \right) - 1 \right) \tag{3.21}$$

where k is Boltzmann constant $\left(1.3806503 \times 10^{-23}\ \mathrm{J/K}\right), q$ - electron charge $\left(1.602179 \times 10^{-19}\mathrm{C}\right)$. PV current I_{ph} depends on module temperature and incident irradiance as per Equation 3.22, whereas, diode saturation current I_0 is influenced by temperature only as given in Equation 3.23. For these calculations values usually provided in PV modules datasheets as measured under standard test conditions (STC) are used: G_{STC} - STC irradiance, $T_{m(STC)}$ - module standard operating temperature, $I_{sc(STC)}$ - short circuit current, $V_{oc(STC)}$ - open circuit voltage. Also, to simplify the calculation, open circuit voltage and short circuit current coeficients (K_V in V/K and K_I in A/K respectively) are utilized. STC values, that were used to produce required I-V curves in this study, are given in Table 3.1.

$$I_{ph} = \left(I_{sc(STC)} + K_I \Delta T \right) \frac{G_{inc}}{G_{STC}} \tag{3.22}$$

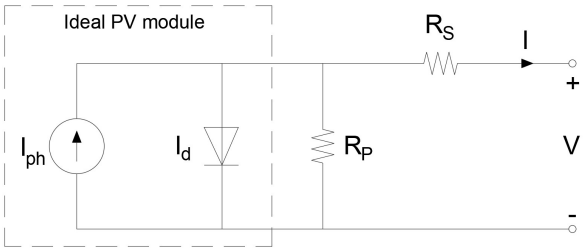

Figure 3.5: Single diode model of a PV cell [43]

$$I_0 = \frac{I_{\mathrm{sc(STC)}} + K_I \Delta T}{\exp\left(\left(V_{oc(STC)} + K_V \Delta T\right)/a_{id} V_t\right) - 1} \tag{3.23}$$

where ΔT is the difference between module temperature T_m and standard operating temperature $T_{m(STC)}$.

Table 3.1: Module parameters used in this study

Parameter	Value
Maximum power (P_{MPP})	400 W
Maximum power voltage (V_{MPP})	42.0 V
Maximum power current (I_{MPP})	9.53 A
Maximum power voltage (V_{MPP})	42.0 V
Open circuit voltage (V_{oc})	49.6 V
Short circuit current (I_{sc})	10.16 A
Cell type	Mono-crystalline
Number of cells	144
Diode ideality constant (a_{id})	1.38
Nominal operating temperature ($T_{m(STC)}$)	41 °C
Voltage temperature coefficient (K_V)	-0.28 %/K
Current temperature coefficient (K_I)	0.05 %/K

3.6 P&O algorithm implementation and experiment

P&O algorithm in this framework is implemented as previously given in Section 2.3. The algorithm implementation is quite straightforward, however, to determine its parameters is not. As discussed in Section 2.3, the range of possible values proposed in the literature is wide and parameter tuning is very important for best algorithm performance. To better understand what parameters are used in real equipment employing MPPT an experiment was carried out. For this purpose a power electronics set-up in the PV lab of the PVMD research group, TU Delft (shown in Figure 3.6) was utilized. As indicated in the figure, equipment used for the experiment was: (1) mini solar simulator and Neste a-Si A13R PV module; (2) digital oscilloscope; (3) solar charge controller (Steca Solarix MPPT 2010); (4) DC-DC disconnector and (5) 12 V 26 Ah ST21 solar battery. Prior to the experiment the exact algorithm implemented in the charge controller was not know, but assumed to be P&O because of its widespread implementation, hence the experiment results only gives an idea of the possible parameters that could be used for P&O implemented in a device. Electrical connections between these devices are given in Figure 3.7.

The purpose of this experiment was to log the voltage curve in time and determine the perturbation step amplitude and sampling period from it. Throughout the duration of the experiment irradiance exposed to the module and the load was kept constant to simulate a steady-state scenario. However, due to the increasing temperature of the module because of incident irradiance and the change in the battery's state of charge, the I-V curves still changed slightly. This is evident in the voltage curve

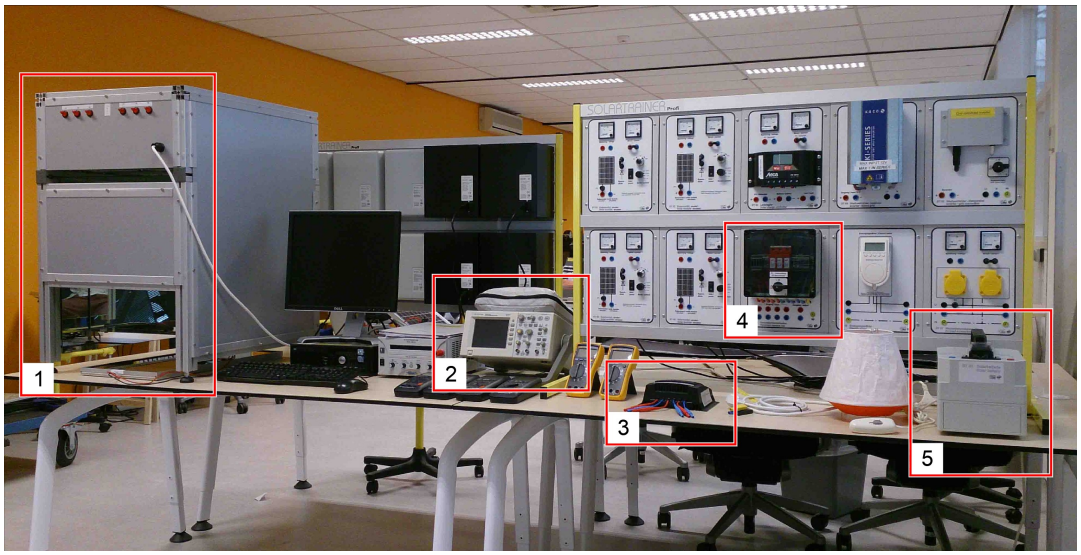

Figure 3.6: Power electronics set-up in PV lab of PVMD research group

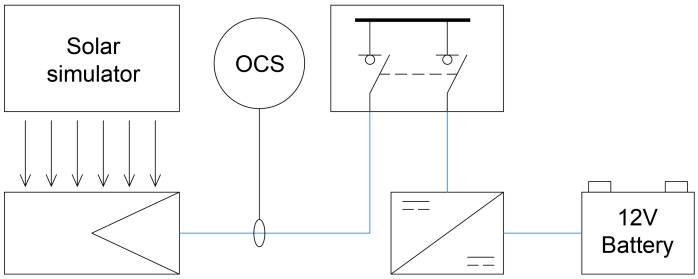

Figure 3.7: Single line diagram of the experimental setup

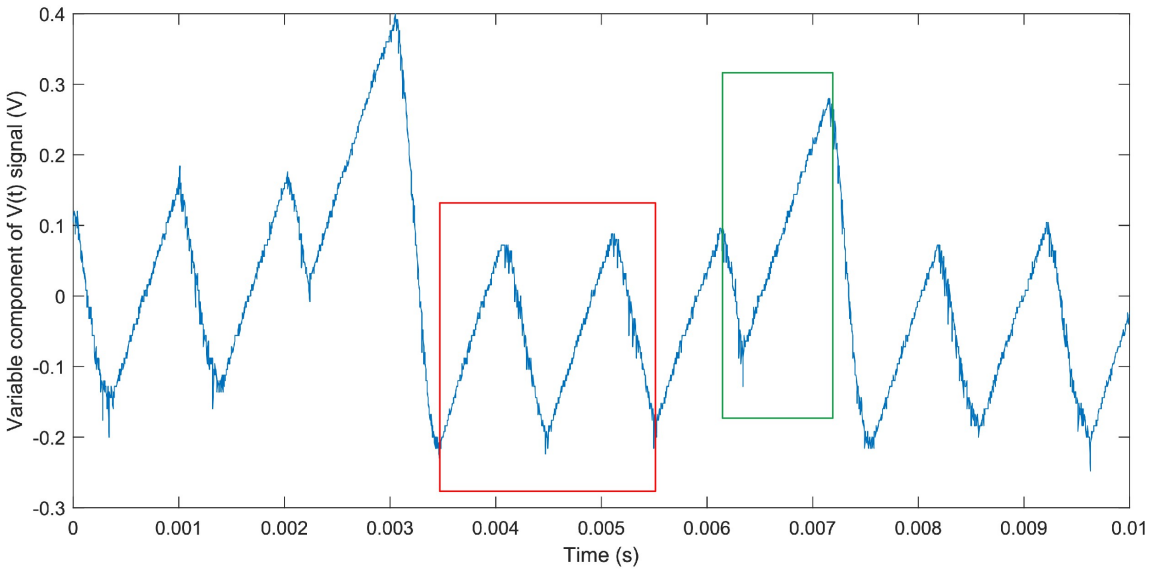

Figure 3.8: Measured operating voltage variable component under stable irradiance

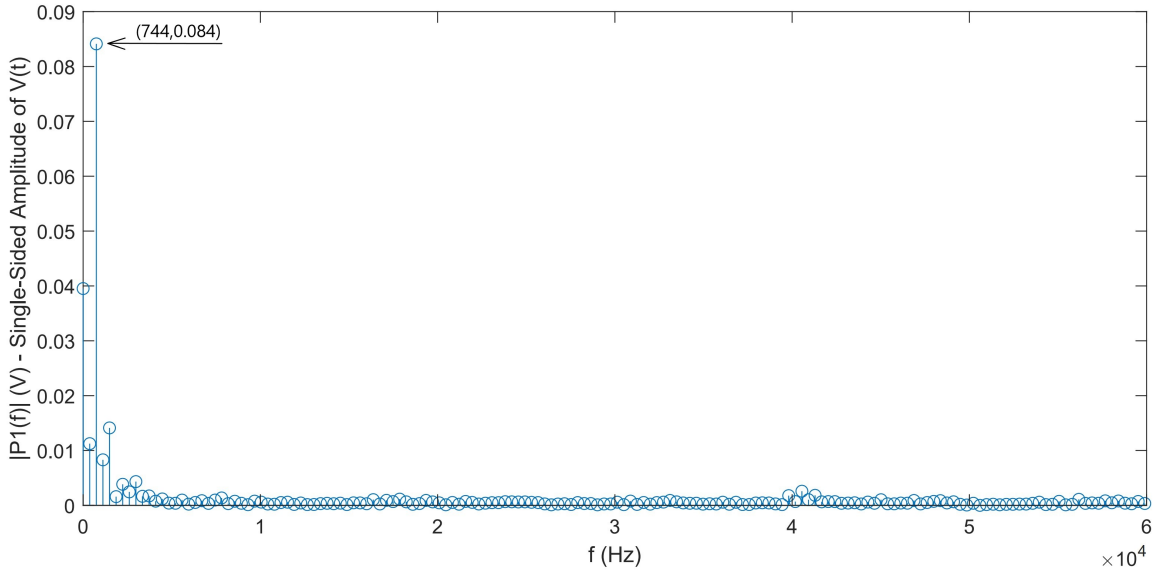

Figure 3.9: Single-sided amplitude spectrum of V(t)

logged by the oscilloscope as shown in Figure 3.8 where steady-state operation of MPPT is marked in red and variable (i.e. when I-V curve changes) - in green. It shows the variable component of the measured operating voltage and the record length is 2500 datapoints taken every 4 µs, thus, 0.01 s in total. Because of such a high rate of data logging, there is noticeable noise present in the signal, however, perturbations can be distinguished easily and P&O parameters are obtained.

While the parameters could be obtained by visibly inspecting the operating voltage signal, a more precise approach was taken. For the steady-state operation part of the signal (0.0035 s to 0.0055 s) a Fourier transform was run (using fast Fourier transform function in Matlab) to acquire the frequency spectrum as shown in Figure 3.9. It can be observed that there is one most prevalent frequency within the signal - 744 Hz - with a respective single-sided amplitude of 0.084 V. In simple terms, the single-sided amplitude is half the amplitude of the periodic signal. Fourier transform obtains frequency values of the harmonics composing a periodic signal - a signal which repeats its values after every fixed period of time. In Figure's 3.8 section of the signal marked in red two such periods are visible. The most dominant 744 Hz frequency is judged to be frequency of these two periods because while there are other harmonics with both higher and lower frequencies in this part of the signal, they are caused by the noise within the logged data and are of no interest. However, this obtained frequency is a measure of the part of the signal Fourier transform was run for, and not of the P&O sampling frequency.

Once the frequency and amplitude of the periodic change of voltage curve was known, it was necessary to determine how this periodic behaviour relates to perturbations made by the algorithm so that algorithm parameters could be obtained. As discussed in Section 2.3, during steady-state operation P&O algorithm finds the maximum power point (or a point close to it) and oscillates around it as was given in Figure 2.7. In time series such oscillations result in a periodic voltage signal, where four perturbations compose one full period of voltage change. With this relation, it can be concluded that the P&O sampling interval T_a is one fourth of the period found from the experimental data log and is equal to 0.000335 s or 0.3 ms (since 744 Hz is 0.00134 s). The full period of voltage change includes two positive and two negative perturbations and hence the amplitude of the full periodic change (full-side amplitude) is two perturbation amplitudes. In other words, one perturbation amplitude is equal to the single-side amplitude of the voltage period, hence, perturbation step amplitude is found to be 0.084 V or 0.6 % of $V_{oc(STC)}$ of the PV module.

The obtained sampling interval value falls on the very low end of the range of values found in literature, while perturbation step amplitude is somewhat average. This does not offer conclusive results that such parameters would be used in real-world scenarios. With the understanding that these parameters

play an important role in P&O performance and should be optimised, a sensitivity study was deemed necessary. It was performed by running the model while varying both perturbation amplitude and period and expanded to include variability of the irradiance as well. This is further discussed in section 4.4.

Another thing to notice when talking about the sampling interval of the P&O algorithm is that it is much smaller than the sampling interval of the data from Oahu, Hawaii. It was already discussed that irradiance data are resampled to have the same temporal resolution as P&O sampling period assuming that irradiance changes linearly. However, this removes any variability occurring between the two irradiance datapoints. If the 3 s data resampling was done so that there was a new point every 0.3 ms, an approximation that 9999 points are increasing/decreasing linearly would be made. In such a case, P&O algorithm would perform in close to steady-state conditions at all times because at each sampling time changes in I-V curves would be minor even during significant irradiance ramping events. Considering this, for the main part of this research a sampling interval of 50 ms was chosen instead and only 59 points were interpolated linearly between the obtained incident irradiance datapoints. While this still is a limiting assumption for the P&O efficiency estimation, the effect of interpolating 59 points instead of 9999 is certainly smaller. To come back to the original resolution of measured irradiance, efficiency values are averaged for each 3 s period and stored together with the irradiance data.

3.7 Irradiance variability metrics and classification

To study P&O efficiency in reference to irradiance variability the variability must be quantified using selected metrics. Since variability is a measure of changes happening within a certain period the metrics are calculated for a period of time. In this case, 1 min period was selected, giving a bin that contains 20 irradiance points. Two types of variability metrics are used: one deterministic (VI) and six statistical. As discussed in Section 2.5, VI is the ratio of the measured irradiance curve within a selected period to the clear-sky irradiance curve in that same period. While this metric has the drawback of having different scale of values when calculated using irradiance data with different temporal resolutions, it was selected because of its simplicity and the unique insight it gives. Three of the statistical metrics utilized in this analysis are based on standard deviation which is a direct description of the variation or dispersion of a given set of values (in this case the 20 datapoints within a minute). This quantifier was selected since it is a widely used metric in many fields of research and is utilized in describing irradiance variability as well. Standard deviations of increments of clear-sky index (Δk_c), increments of clearness index (Δk_t) and irradiance ramp rates (r) were selected as three of the six statistical features. Increments are defined as the absolute change between subsequent values (Equation 3.24), whereas irradiance ramp rate is a change of irradiance per second of time (Equation 3.25). Calculation of standard deviation is given in Equation 3.26 [10] taking Δk_t as an example. In addition, simple statistical metrics like mean, maximum and minimum values of ramp rate within the selected period time are used which allows for a full description of the distribution of ramp rate values within that period. The full set of variability metrics is given in Table 3.2.

$$\begin{aligned} \Delta k_{t,i} &= k_{t,i+1} - k_{t,i} \\ \Delta k_{c,i} &= k_{c,i+1} - k_{c,i} \end{aligned} \tag{3.24}$$

$$r_i = \frac{GHI_{i+1} - GHI_i}{\Delta t} \tag{3.25}$$

where Δt is the irradiance data sampling interval (3 s in this case).

$$\sigma\left(\Delta k_t\right) = \frac{1}{N}\sqrt{\sum_{i=0}^{N}\left|\Delta k_{t,i}\right|^2 - \left(\sum_{i=0}^{N}\left|\Delta k_{t,i}\right|\right)^2} \tag{3.26}$$

where N is number of data points in a time interval for which σ is computed.

Table 3.2: Variability metrics used in the analysis of P&O efficiency relation to irradiance variability

Name	Symbol
Variability index	VI
Standard deviation of clear-sky index increments	$\sigma(\Delta k_c)$
Standard deviation of clearness index increments	$\sigma(\Delta k_t)$
Standard deviation of irradiance ramp rate	$\sigma(r)$
Maximum ramp rate	$max(r)$
Minimum ramp rate	$min(r)$
Mean ramp rate	$\mu(r)$

Furthermore, to get more understanding about the irradiance conditions from the data other than what is provided by the previously discussed metrics, a period of time could be classified in terms of its variability. There are many methods proposed, however, to have the largest number of classes and for the simplicity of calculations (and hence low computation resources necessary for it) a deterministic approach using VI and k_c values were undertaken [44]. This method is usually utilized to classify days into five categories: clear, overcast, highly variable, moderately variable and mildly variable. The algorithm of categorization is given in Equation 3.27. However, it must be noted that VI values in Equation 3.27 are obtained when computed using 1 min irradiance data. Here the shortcoming of VI as a metric can be highlighted since there is no straightforward relation between VI values when computed using data with different temporal resolutions. This can be explained by the fact that one minute irradiance data are averages of higher resolution data and this higher resolution can not be recreated. The same is with VI values - if it is calculated for 1 min resolution it is very difficult to guess what kind of variability 'lies within' this value at higher resolution. Additionally, as was discussed in Section 2.5, the value of VI depends on the resolution of the data used because of the VI equation itself and its physical meaning. VI is the ratio of the length of GHI curve and length of the clear-sky irradiance curve. Using higher resolution of data will increase the length of GHI curve (since more variability will be present) while clear-sky irradiance curve length will not change. This way the VI will have larger values. Because of this, when days (or later, hours - explained in Section 4.4) are being classified, VIs must be recalculated using 1 min averages of the 3 s data.

$$\begin{cases} \text{Clear if } \begin{cases} k_c \geq 0.5 \\ VI < 2 \end{cases} \\ \text{Overcast if } \begin{cases} k_c < 0.5 \\ VI < 2 \end{cases} \\ \text{Mild if } 2 \leq VI < 5 \\ \text{Moderate if } 5 \leq VI < 10 \\ \text{High if } 10 \leq VI \end{cases} \tag{3.27}$$

4

Results

The methodology explained in Chapter 3 was used to prepare a dataset containing original irradiance measurements sampled every 3 s and computed average P&O efficiency values within respective 3 s periods. The 3 s data was then used to produce datasets comprising irradiance variability metrics at a resolution relevant to specific analysis done and average P&O efficiency values to match the resolution of variability metrics. In this chapter, an analysis of the data and its results are presented. Firstly, the prepared dataset is introduced in Section 4.1. Then the data exploratory analysis to answer the proposed research questions is discussed starting with the investigation of P&O efficiency changes on a monthly and daily basis as demonstrated in Section 4.2. Then the analysis is focused on an intra-day 1 min scale to determine the relationship between P&O efficiency and variability metrics and is given in Section 4.3. Lastly, a sensitivity study was performed to investigate the effects of parameter selection on the efficiency depending on the variability of irradiance. This is showcased in Section 4.4.

4.1 Dataset overview

The 3 s dataset was prepared following the methodology explained in Chapter 3 and comprised of the computed P&O (with $T_a = 50ms$ and $\Delta V = 0.6\%$ of $V_{oc(STC)}$) efficiency and the irradiance values. In order to describe the irradiance conditions, three quantifiers - clear-sky index (k_c), clearness index (k_t), ramp rates (r) - were calculated for further analysis. All the features contained in the dataset are presented in Figure 4.1 for a non-variable (4.1a) and a variable (4.1b) irradiance day. In the first case, the measured GHI curve follows a similar trend as the one of clear-sky irradiance (G_c), yet GHI values are lower than G_c which indicates that during this day there was a relatively uniform and continual cloud cover present. Also, it can be observed that the irradiance curve fluctuates only in the second half of the day as seen more profoundly in the k_c and k_t values. However, these fluctuations do not result in high ramp rates - a maximum of around 10 W/m^2/s is observed. Major drops in P&O efficiency are also absent, it stays very close to 100% throughout the day. On the other hand, during variable day observed GHI does not resemble clear-sky irradiance and instead shows major variance in irradiance and k_c, k_t values. This suggests that during this day there was a substantial scatter and movement of clouds that resulted in obstruction of the sun and hence considerable fluctuations of measured irradiance can be observed. As ramp rates quantify the variance of irradiance, these values are also substantially higher reaching up to 200 W/m^2/s. In such cases, drops in efficiency down to less than 90% are present, which suggests the dependency of P&O efficiency on the variability of irradiance.

In this thesis, the relationship between P&O algorithm efficiency and irradiance variability is studied using variability metrics which are computed to represent variability within a 1 min period as proposed in Section 3.7. The 3 s data was used to calculate seven variability metrics: VI, standard deviations of k_c increments, of k_t increments and of ramp rates, as well as maximum, minimum and mean ramp rates for each 1 min period. Figure 4.2 shows the 1 min average P&O efficiency in comparison with all seven variability metrics and it can be observed that the trends are different. For example, there is a greater dispersion of efficiency values at larger standard deviations of Δk_c and Δk_t, but such trend is weaker in case of standard deviation, maximum and mean of ramp rate, and opposite when studied against VI and minimum ramp rate. Additionally, Figure 4.2 shows outliers - data points further away from the main cluster. Since the aim of this study is to determine a relationship between P&O efficiency and these metrics, from a data analysis perspective it would be beneficial to filter them out. However, due to the lack of a definitive methodology for filtration, the dataset was analyzed in its original form. It

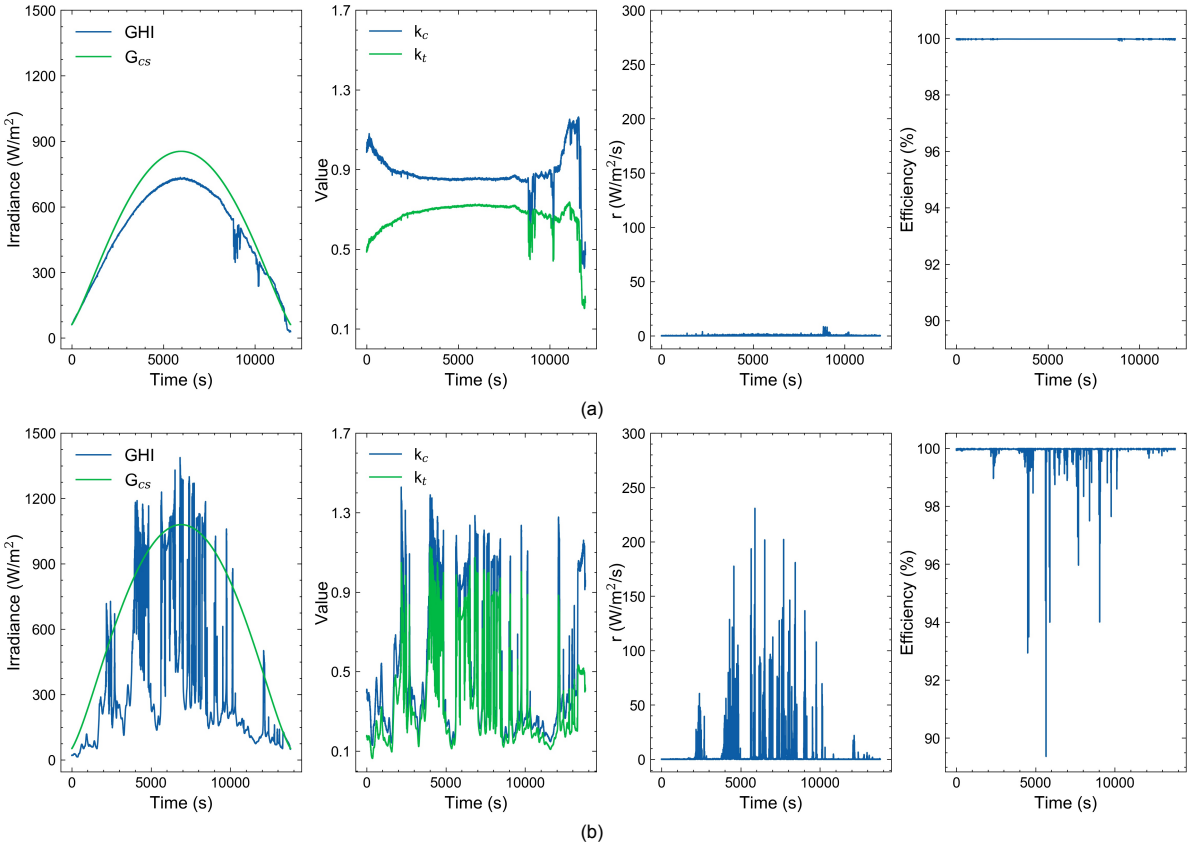

Figure 4.1: 3 s data representation of (a) a non-variable irradiance day (07-12-2011) and (b) variable irradiance day (10-09-2010)

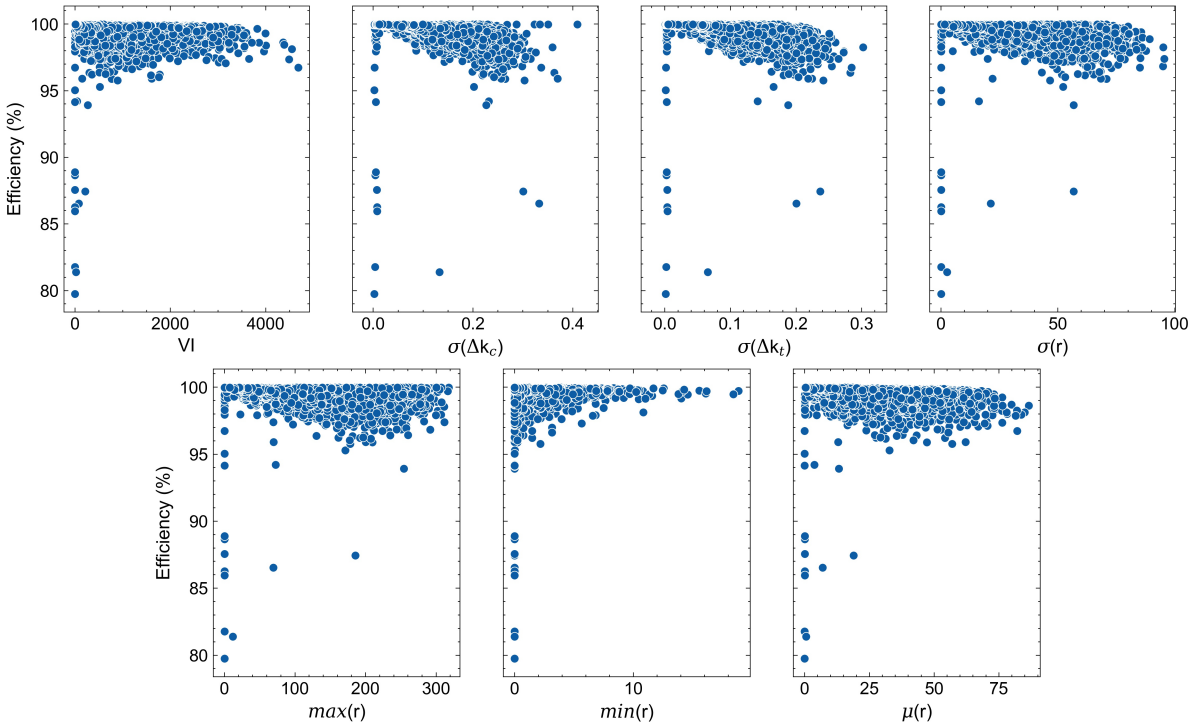

Figure 4.2: 1 min average efficiency against 1 min variability metrics

is also important to mention that for coherence of the analysis, data points when elevation of the Sun is lower than 5° are eliminated.

4.2 Monthly and daily P&O algorithm efficiency

The prepared datasets were firstly analysed on a monthly basis. Figure 4.3 shows average monthly P&O efficiencies from April 2010 to March 2011. In general, the average monthly efficiencies range between 99.908% and 99.964%, so the variation is minor, however, still present. In spring and summer, P&O efficiency is lower when compared to autumn and winter, where the months of December and February show the highest efficiencies. While the monthly variance is interesting to investigate, for example, for the purpose of yield estimations, it does not provide information on the variability of irradiance. Hence, to further examine the reason behind this monthly variation, all days within the year were classified utilizing the deterministic approach based on VI and k_c values as introduced in Section 3.7. For this, the year worth of 3 s irradiance data was re-sampled to 1 min averages and daily values of VI and k_c were obtained. Results of the classification are shown in Figure 4.4. It is evident that most of the days are classified as highly variable, followed by moderate and mild. Only five days were determined to be overcast and ten days - clear. This concludes that in Oahu, Hawaii variability of irradiance is mostly high. Then days from each class within all respective months were counted depending on its class as presented in Figure 4.5. The reason behind winter months having highest efficiencies can be explained by the fact that these months have lowest number of highly variable days. This relates to Köppen-Geiger climate type of Hawaii being an equatorial savanna with dry winter. Months of April to September have mostly highly variable days with a few moderately variable days. However, while July demonstrates the highest P&O efficiency out of these months it is exactly the same in terms of daily variability as August. This indicates that further analysis on a higher temporal resolution of variability is necessary. However, from these observations, it can be concluded that in locations where irradiance variability is mostly high, efficiency loss of up to 0.1% can be estimated on a monthly scale due to the performance of P&O algorithm.

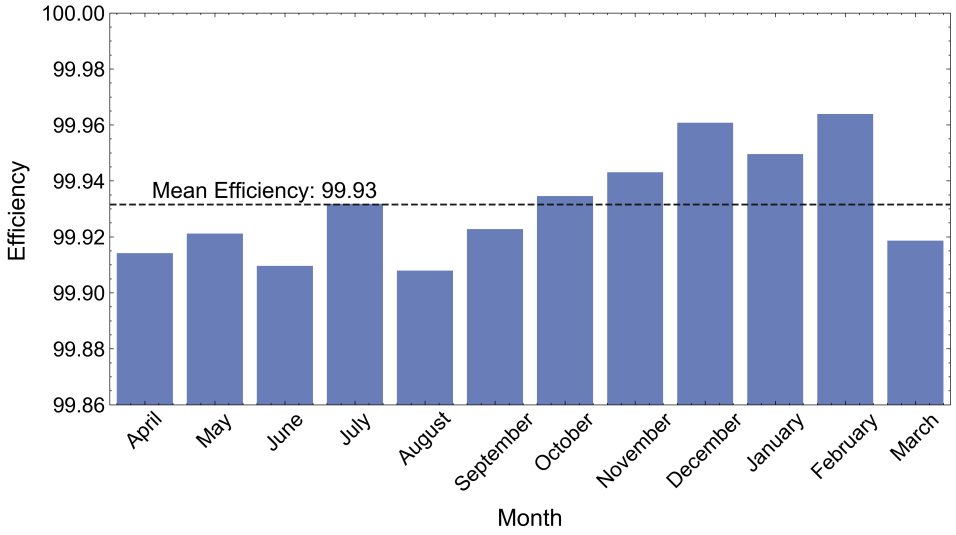

Figure 4.3: Monthly and yearly average P&O efficiency

To further understand the reason behind different monthly efficiencies when the daily variability within them is the same, the P&O efficiency values were studied against the variability class of the day. For this, a daily resolution was introduced and daily average efficiency values were aggregated. It can be observed that efficiency in each class can take a range of values as shown in the box plots in Figure 4.6. This means that two highly variable days can have different P&O efficiencies resulting in different monthly values even when the number of days in each class is exactly the same. Visualising the box plot of daily efficiency values within each class provides more information than just a mean value. In

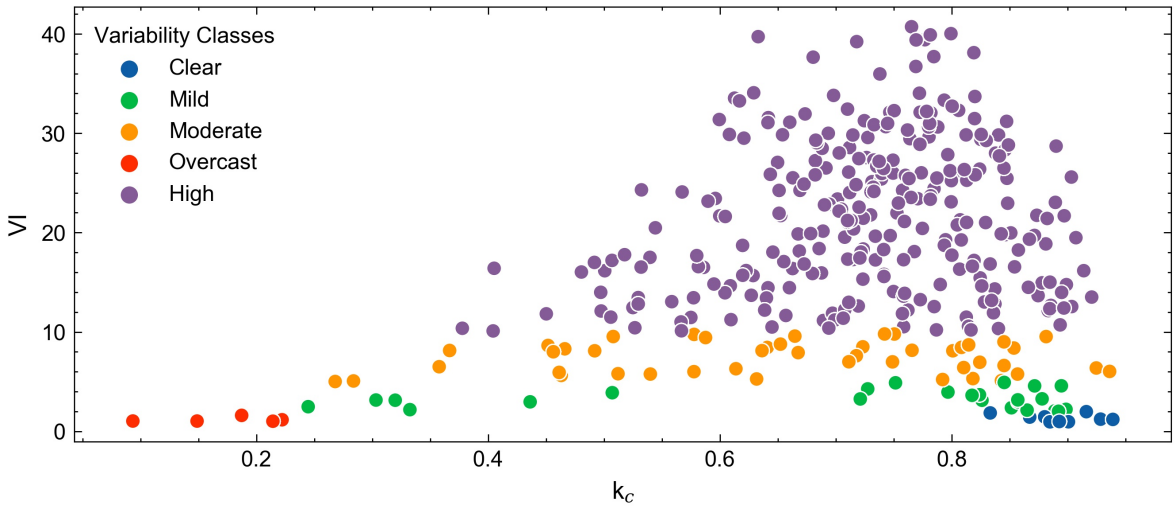

Figure 4.4: Day classification based on k_c and VI

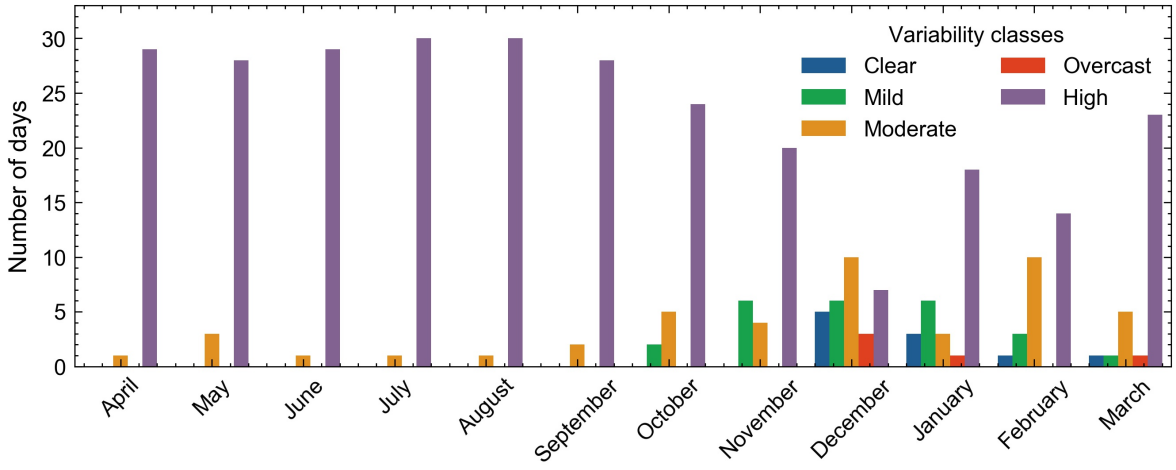

Figure 4.5: Number of days from each variability class during each month of the year

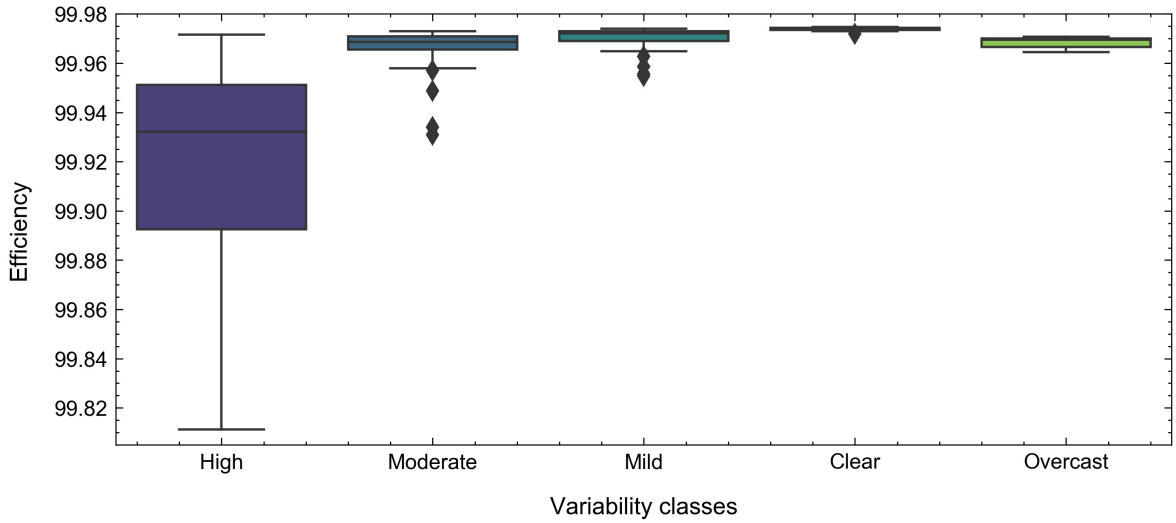

Figure 4.6: Average daily P&O efficiency based on variability class of the day

fact, box plots visually show the distribution of numerical data and aid in understanding the dispersion (also called scatter, variability or spread) of the variable in concern, which in this case is P&O efficiency. The lines within the box give the median value of the efficiency within each respective class and the bottom and top edges of the box represent the 25^{th} (Q_1) and 75^{th} (Q_3) percentiles, respectively. The area inside the box depicts the inter-quartile range (IQR) showing the middle 50% of efficiency values and is expressed as the difference between the lower and upper quartile values ($IQR = Q_3 - Q_1$). The lowest and the highest efficiency values are found at the end of the whiskers which are 1.5 IQR away from the lower and upper quartiles ($Q_1 - 1.5 * IQR$; $Q_3 + 1.5 * IQR$). Additionally, any point which is outside the whiskers of the box plot is termed as outliers and can be seen for mild and moderate variability classes. In this plot, it can be noticed that daily efficiencies have similar values to the monthly ones. However, when irradiance variability during the day is high efficiency values could drop down to 99.82% and lower. Also, efficiency values reduce when the variability of the day increases as general logic would suggest. It is also worth noting that P&O efficiency is lower during an overcast day than during a clear or mildly variable day. However, it should be pointed out that most of the days were classified as highly variable and hence many more efficiency values were available to produce the box-plot for high variability days than any other which reduces comparability to other classes.

4.3 Intra-day irradiance variability and P&O algorithm efficiency

Variability of irradiance usually refers to changes in irradiance due to cloud existence and movement. While cloudiness varies from one day to another, generalising dynamic conditions of cloud movement on a daily basis results in averaging effects of reduced informativeness. To that end, irradiance variability and its effects on P&O within a day were studied using 1 min periods. Firstly, to understand the strength of the relationship between the 1 min variability metrics and 1 min averaged efficiency values Pearson correlation coefficients were calculated. Pearson correlation describes the linear relationship between two variables where the sign of coefficient means the direction of linearity and the magnitude - the strength of relationship, which ranges from 0 (no correlation) to 1 (perfect correlation) [45].

Figure 4.7 shows Pearson correlation coefficient matrix between all variability metrics and efficiency computed for all 1 min periods available in a year. It is evident that all variability metrics are positively correlated between themselves. As k_c and k_t are very similar measures their increments' standard deviations correlate ideally with coefficient values equal to one. These metrics correlate very strongly to all other variability metrics based on ramp rates except for minimum ramp rate, which, in fact, does not have a strong relationship with any other metric. The only deterministic variability metric VI does not correlate to other measures as strongly, which suggests that it provides more or different insight into the variance of irradiance. Lastly, and most importantly, efficiency has a negative correlation to variability metrics indicating that with an increasing variability, efficiency decreases. However, the interrelationship is not strong as magnitudes of Pearson correlation coefficients do not reach 0.3.

The reason behind the weak correlation between P&O efficiency and variability metrics can be explained when inspecting Figure 4.8. For the purpose of example, it shows efficiency values against mean ramp rate providing density of the datapoints as well. It is observed that while there is a general decrease in efficiency when the ramp rate increases the data are largely scattered. This means that many of the data points are far away from the general linear trend of the whole dataset, which in turn results in a weak Pearson correlation. Another reason for the low magnitudes of the Pearson correlation coefficient could be the outliers seen in Figure 4.2. However, the figure shows that most of the efficiency values lie in a range of 98% to 100%, so if one would study only data with efficiency values above 98% most of the information would still be retained. This was done by recalculating Pearson correlation coefficients for variability metrics and efficiency when the latter is more than 98% and is shown in Figure 4.9. In such case, Pearson correlation coefficients are more than two times larger in magnitude when compared to the case when all data are used indicating a stronger relationship. However, the coefficients still do not reach 0.7 and the relationship cannot be characterised as strong. Additionally, the efficiency to minimum ramp rate correlation coefficient is still under -0.25 suggesting a very weak relation, and therefore minimum ramp rate was not used for any further analysis.

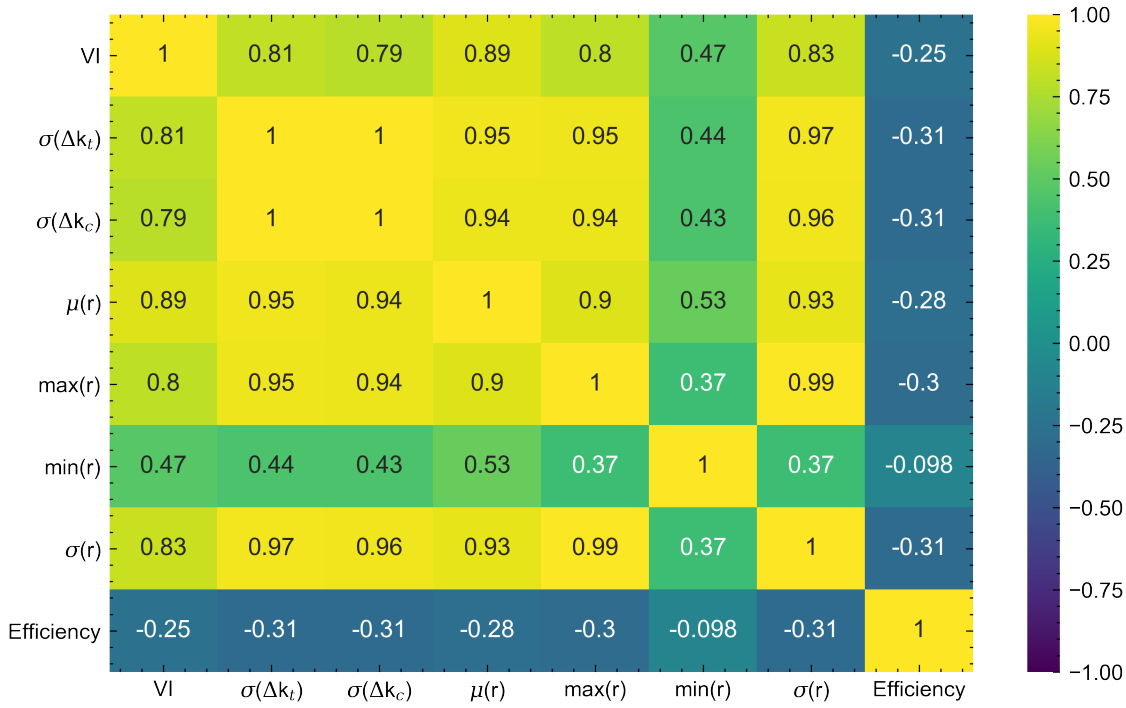

Figure 4.7: Pearson correlation coefficients between 1 min resolution variability metrics and 1 min average P&O efficiency during the year

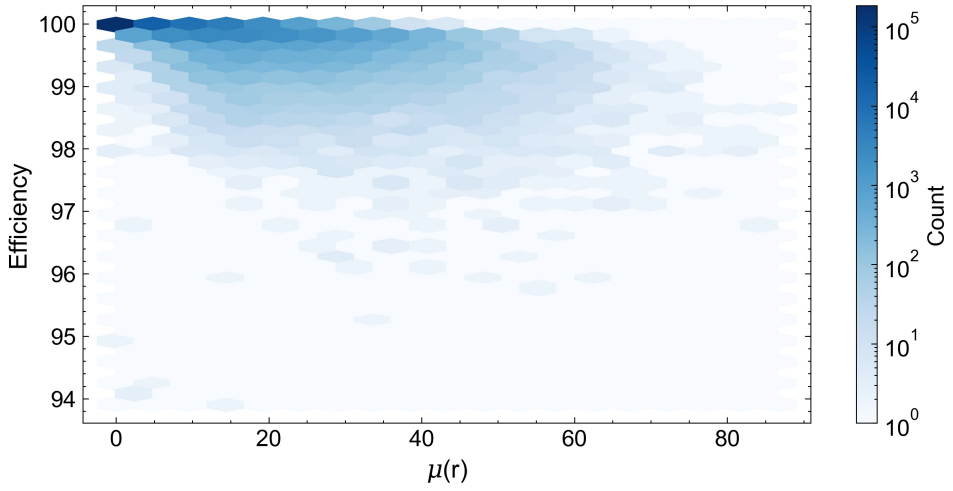

Figure 4.8: 1min P&O efficiency against ramp rate and density of data

Because of the relatively weak correlation between individual 1 min average efficiency values and variability metrics within respective periods, quantifying the efficiency dependence on variability directly from the produced 1 min dataset was determined to be ineffectual. Instead, the variability metrics were segregated into 50 bins and the average efficiency for each bin was obtained. This provides an estimate of what 1 min average efficiency could be expected depending on variability quantified by a specific metric. To quantify the relationship, curve fitting through the binned and averaged efficiency data was done. The generic function of curve fit is described by the equation $y = p_1 * x^2 + p_2 * x + p_3$. The efficiency data and curves fitted through it are shown in Figures 4.10 and 4.11. VI, maximum and mean ramp rate was determined to be related to efficiency linearly, while standard deviations of k_c, k_t increments and ramp rate - quadratically. Function coefficients of the curve fit for each of the variability metric and P&O efficiency pairs are given in Table 4.1. To conclude, these obtained functions describe the relationship between variability and P&O efficiency and they can be used to estimate P&O

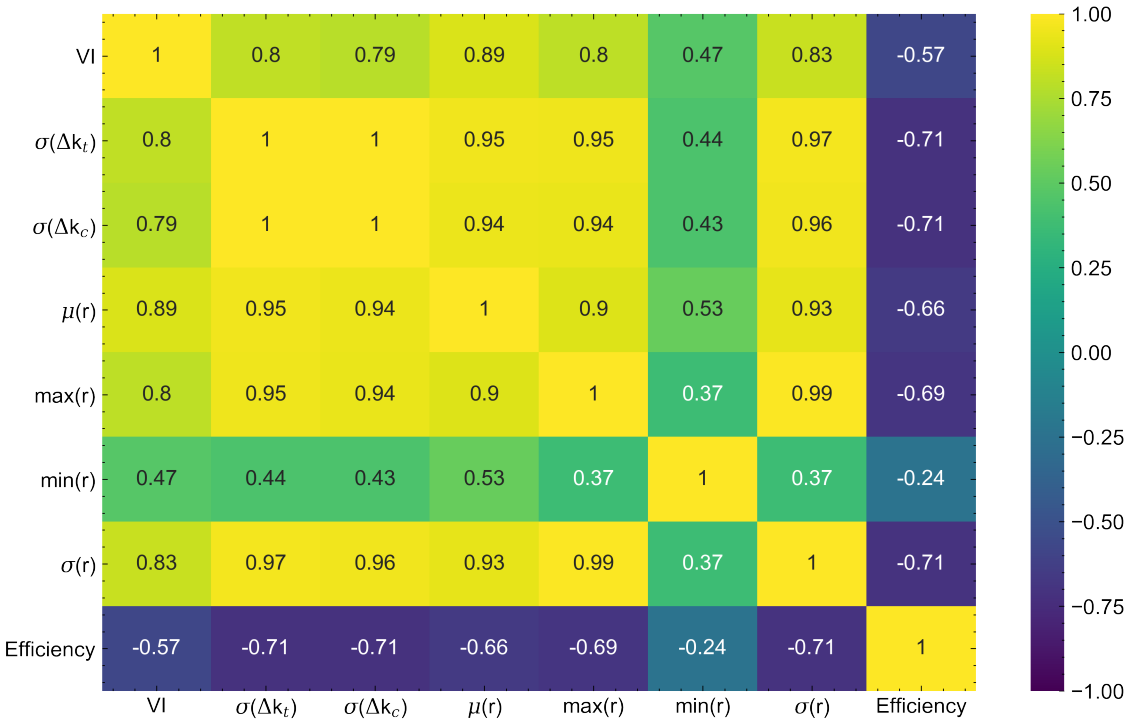

Figure 4.9: Pearson correlation coefficients between 1 min average P&O efficiency higher than 98% and respective 1 min resolution variability metrics

efficiency value when one of the six 1 min variability metrics are known. Since these variability metrics can be computed using high temporal resolution irradiance data and does not depend on where the data was collected, the functions of P&O efficiency and variability relationships could be applied to any location. However, magnitudes of the variability metrics depend on data sampling frequency which will be discussed further in Chapter 5. Hence, one should be cautious when estimating efficiency with the defined functions and using variability metrics computed using data of different resolution than 3 s.

The curve fits were tested for their goodness and in turn for their approximation certainty. In addition to the curve function parameters, Table 4.1 demonstrates the goodness-of-fit metrics: R^2, root mean squared error (RMSE) and Kolmogorov-Smirnov statistic. R^2 is the coefficient of determination and in practical terms describes the fraction of total datapoints that can be explained by the proposed curve fit. It's value ranges from 0 to 1 and higher values signify a better fit. The table presents that R^2 values for all of the variability metrics to efficiency pairs are higher or equal to 0.82 indicating relatively good fits in all cases. RMSE is a measure describing the average distance between the data points and curve fit, so the smaller it is the better the fit; its magnitude depends on the values in the dataset. Largest RMSE values are obtained for the curve fits when variability metric is standard deviation of k_c increments, standard deviation of ramp rate and mean ramp rate. However, it must be noted that range of mean efficiency values within bins are larger than in other cases. For example when studied against mean ramp rate average efficiency drop to just above 97.5% when the mean ramp rate is high, whereas efficiency reduces only to 99% when the maximum ramp rate exceeds 250 W/m^2/s. To that end, a normalization of RMSE is proposed and is based on the range of available mean binned efficiency values (max(Efficiency) - min(Efficiency)) which allows for better comparison. Subject to normalised RMSE best fit is determined for efficiency values against $\sigma(\Delta k_t)$ and worst - against max(r). Lastly, the Kolmogorov-Smirnov (K-S) statistic was evaluated which gives insight into how similar the curve is to the data in terms of their probability distributions. It signifies the maximum distance between cumulative distribution functions (CDF) and can have values between 0 (no difference between CDFs) and 1 (maximum difference between CDFs). $\sigma(\Delta k_t)$, σ(r) and max(r) show the best K-S test results. Overall the best curve fit is accomplished for the standard deviation of clearness index increments $\sigma(\Delta k_t)$, however, all curves were concluded to be appropriate for approximating 1 min average efficiency values.

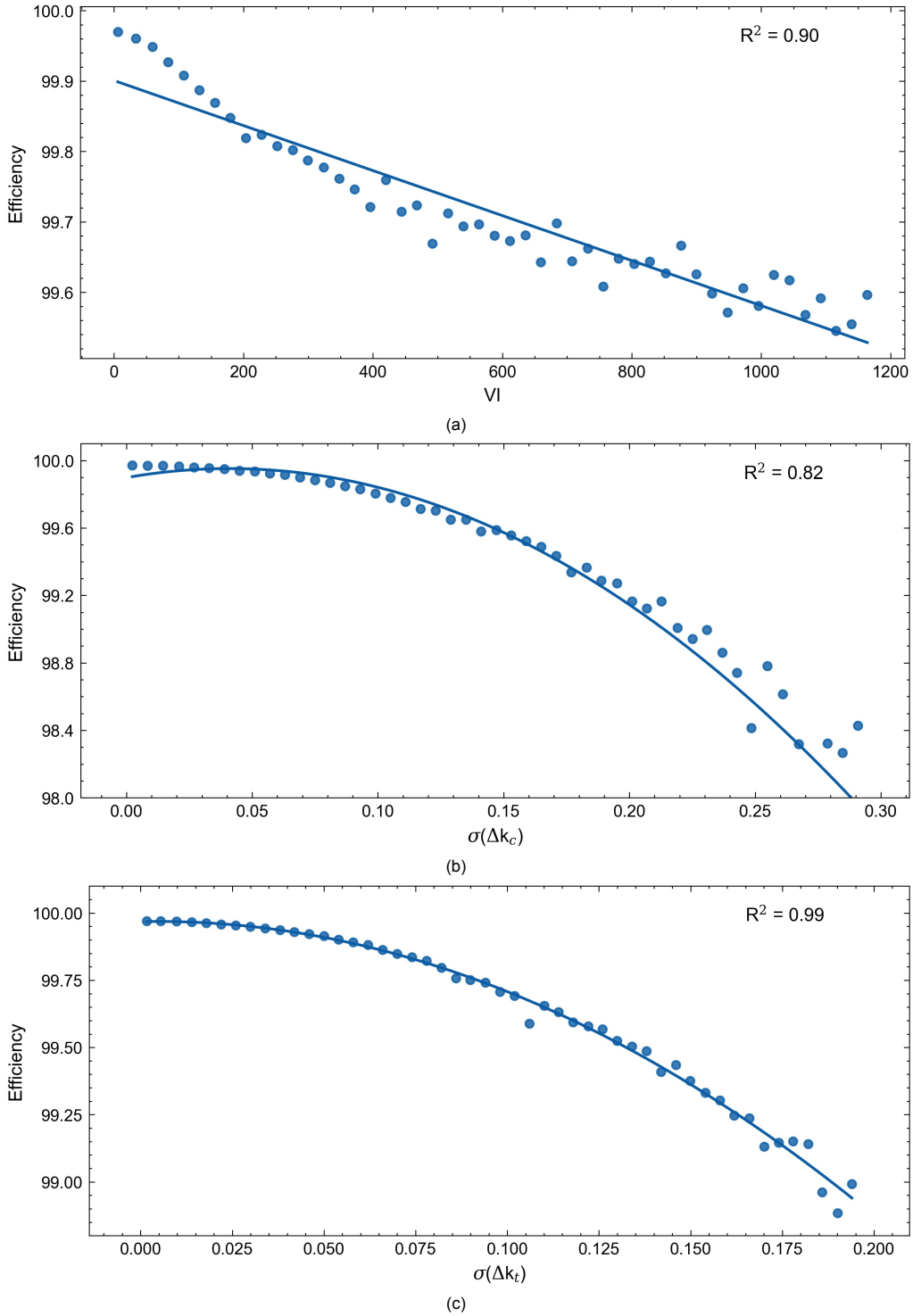

Figure 4.10: Mean P&O efficiency within bins of (a) variability index, (b) standard deviation of k_c increments, (c) standard deviation of k_t increments

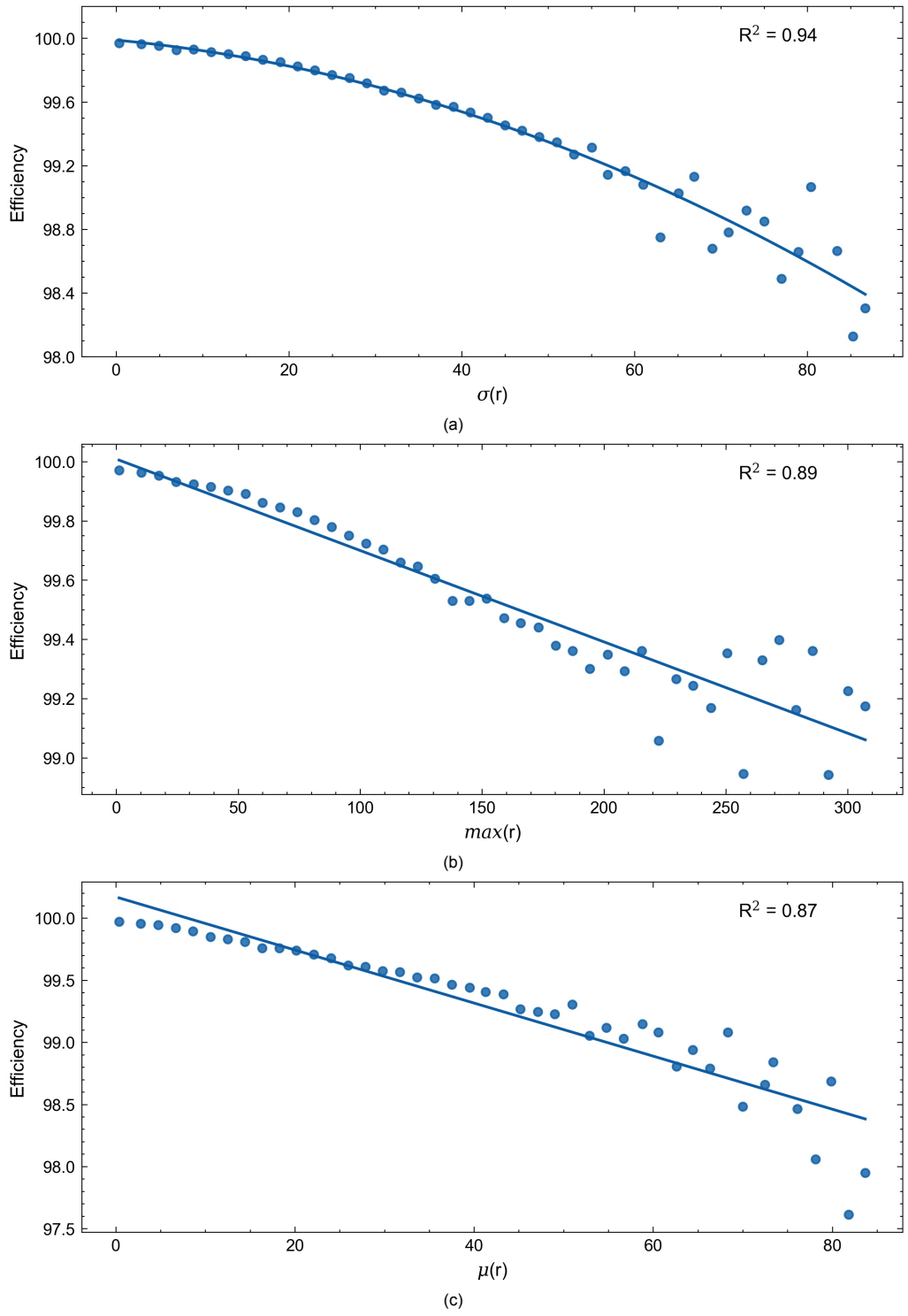

Figure 4.11: Mean P&O efficiency within bins of (a) standard deviation of ramp rates, (b) maximum ramp rate, (c) mean ramp rate

Table 4.1: Curve fit function parameters and goodness-of-fit metrics

Variability metrics	p_1	p_2	p_3	R^2	RMSE	NRMSE	KS
VI	0	-3.23x10^{-4}	99.90	0.90	0.035	0.083	0.12
$\sigma(\Delta k_c)$	-31.94	2.62	99.89	0.82	0.28	0.079	0.12
$\sigma(\Delta k_t)$	-28.67	0.26	99.89	0.99	0.028	0.026	0.06
σ(r)	-1.53x10^{-4}	-5.1x10^{-3}	99.98	0.94	0.12	0.066	0.04
max(r)	0	-3.1x10^{-3}	99.99	0.89	0.096	0.094	0.07
μ(r)	0	-0.02	99.97	0.87	0.19	0.085	0.11

4.4 Sensitivity of P&O algorithm efficiency to its parameters

As discussed in Section 2.3, parameters of P&O algorithm highly influence the performance and efficiency of the algorithm. While there is a methodology proposed on how to tune the parameters depending on the electrical components of the system and maximum ramp rate occurring during the sampling period [8] (discussed in Section 2.3), there is no study examining effects of varying sampling interval and perturbation step amplitude on the efficiency of the P&O algorithm depending on the variability of irradiance. Here variability is referred to as descriptive of real-world irradiance conditions on a larger time span than a few seconds. Hence, the sensitivity study as discussed in this chapter aims to fill this gap in the literature.

To perform the sensitivity analysis, firstly, a number of sampling period and perturbation step amplitude values were selected based on the range of such values found in the literature (as summarised in Table 2.2). Seven T_a and seven ΔV values are used in this study as shown in Table 4.2 which when combined results in 49 pairs of parameters. The model was run to produce new datasets when using each of these parameter pairs. The time range for which the model was to be run had to be equal in all scenarios for purpose of comparability, however, it was not realistic to recompute the datasets with each pair of parameters for the entire year. In Section 3.5 it was explained that it is necessary to approximate irradiance values at each step of perturbation because irradiance data are sampled at a lower resolution of 3 s. In this study minimum sampling period is 0.1 ms which means that in such a case between each 3 s values 30000 irradiance datapoints must be created, I-V curves computed and the operating point determined. Even running such simulation for a day would result in hundreds of millions of data points for which extensive computing power is required. Thus, sensitivity analysis was done by taking 1 hour of irradiance values instead. Five different hours were selected depending on their variability - one from each variability class. A random day from each variability class was taken and the same hour - between 12 and 13 o'clock - was selected. The hours were also tested to see if they comply with the variability classes they represent taking their hourly VI and k_c values and using the same criteria for classification as mentioned in Section 3.7. These are presented in Table 4.3. In conclusion, the simulations were done 245 times - using 49 pairs of parameters for each of the 5 selected hours.

Table 4.2: P&O parameters selected for sensitivity analysis

T_a (ms)	0.1	1	10	50	100	500	1000
ΔV (% of $V_{oc(STC)}$)	0.1	0.2	0.3	0.6	1	2	3

In order to understand the relationship between P&O efficiency and its parameters (T_a and ΔV), tricontour plots for all five classified hours were plotted, as shown in Figure 4.12. From initial observation, it can be seen that the P&O efficiency varies with change in P&O parameters, for all variability classes. This can be seen as the change in colour gradient, where yellow represents high efficiency values ($\geq$ 99.9%) and tends towards blue as the efficiency decreases. Although no two variability classes show the exact same contours, it can be observed that the hours classified as clear (4.12a), mild (4.12c) and moderate (4.12d) demonstrate a similar relationship between P&O efficiency and parameters. In all three cases, high efficiency values are recorded for all sampling periods when ΔV is less than or equal to 1.2% of $V_{oc(STC)}$. However, the efficiency decreases uniformly across all sampling periods

Table 4.3: Variability classification based on VI and k_c values for five different days in the hour between 12 and 13 o'clock

Date	VI	k_c	Variability class
25-01-2011	1.22	0.58	Clear
10-01-2011	1.81	0.09	Overcast
24-03-2011	2.58	0.78	Mild
28-06-2010	6.63	0.22	Moderate
01-01-2011	16.8	0.89	High

as the ΔV increases. This can be explained by the fact that in relatively steady-state conditions larger perturbation step size results in larger oscillations around the MPP, which in turn is characterised by a decrease in P&O efficiency. It is interesting to note that the minimum efficiency for both clear and mild classified hours is observed at a sampling period of 0.1 s and perturbation step in the zrange of 2.7 - 3% of $V_{oc(STC)}$. However, for the same range of ΔV, the efficiency improves as T_a increases from 0.1 s to 1 s.

Figure 4.12 (b) shows the contour plot for the hour classified as overcast. Although the trends in efficiency are similar to the ones observed previously (for all sampling periods, a decrease in efficiency is observed as ΔV increases), there is an intriguing behaviour in the region defined by high sampling periods (0.1 - 1 s) and low ΔV values (0.1 - 0.5% of $V_{oc(STC)}$). Contrary to the previously seen behaviour, the efficiency decreases as the ΔV decreases from 1 to 0.1% of $V_{oc(STC)}$. Such a trend is even more evident for the highly variable hour (Fig. 4.12e), where the decrease in efficiency with decreasing ΔV is visible for sampling periods from 0.01 to 0.1 s. However, for the high variability hour, a general decrease independent of the perturbation step size in efficiency is observed when T_a exceeds 0.1 s, but the lowest efficiency is present when the sampling interval is 1 s and perturbation step amplitude is around 1 % of $V_{oc(STC)}$. In general, it can be seen that the P&O efficiency is more sensitive to its parameters as the variability in irradiance increases. It can also be concluded that efficiency will be high in any variability conditions when ΔV is kept below 1 % of $V_{oc(STC)}$ and T_a - below 10 ms. However, it must be noted that a minimum T_a should be established depending on the topology of the converter so that algorithm failures due to transient behaviour would be avoided.

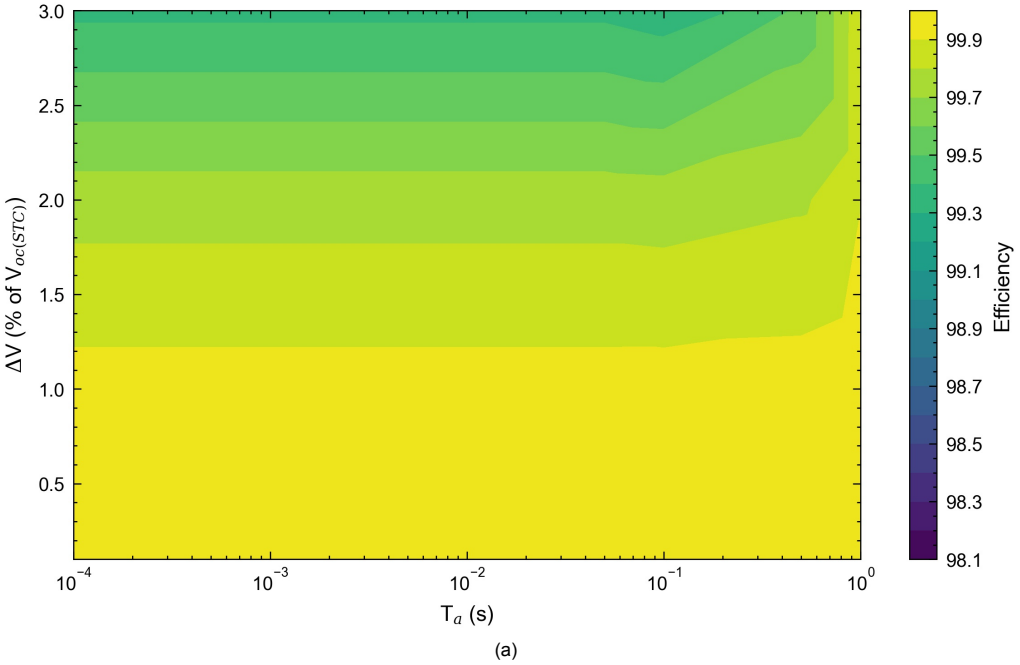
3.0
2.5
2.0
1.5
1.0
0.5
ΔV (% of V$_{oc(STC)}$)
10^{-4}
10^{-3}
10^{-2}
10^{-1}
10^{0}
T$_a$ (s)
99.9
99.7
99.5
99.3
99.1
98.9
98.7
98.5
98.3
98.1
Efficiency

(a)

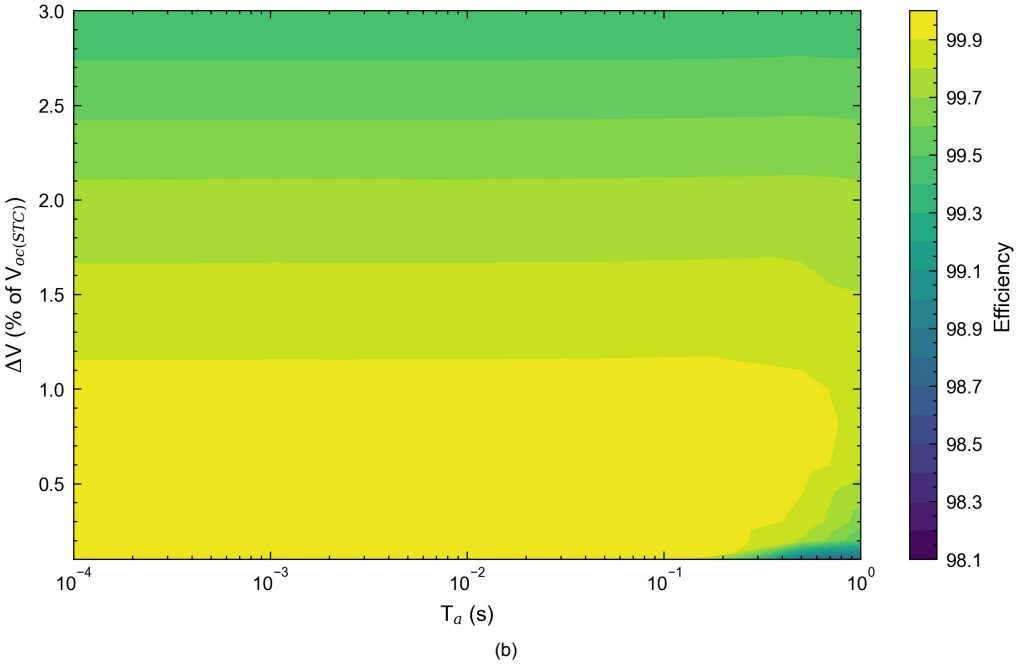
3.0
2.5
2.0
1.5
1.0
0.5
ΔV (% of V$_{oc(STC)}$)
10^{-4}
10^{-3}
10^{-2}
10^{-1}
10^{0}
T$_a$ (s)
99.9
99.7
99.5
99.3
99.1
98.9
98.7
98.5
98.3
98.1
Efficiency

(b)

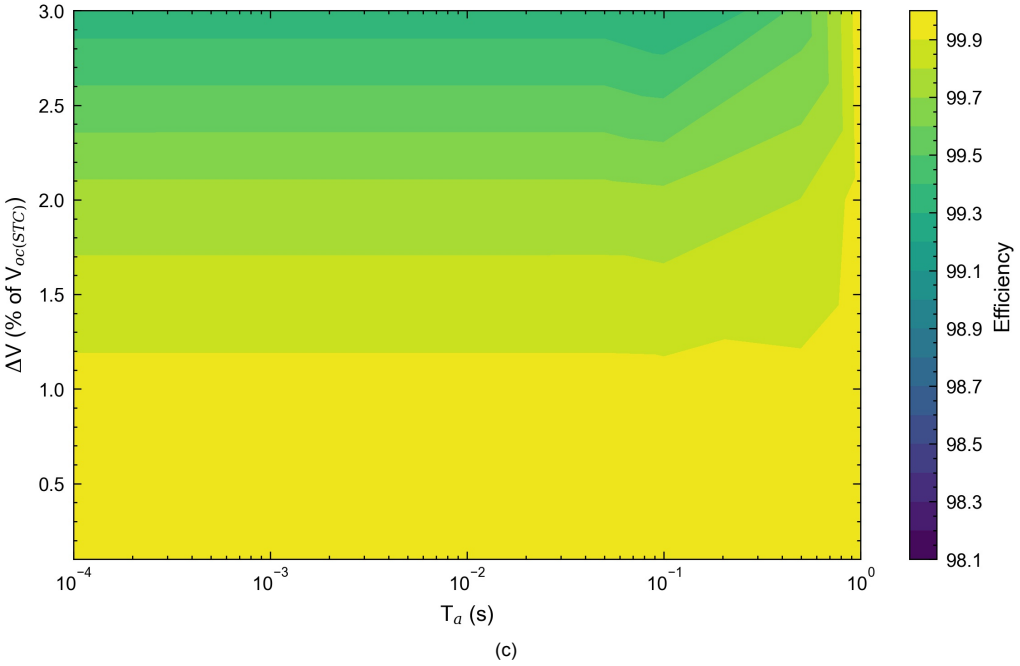
3.0
2.5
2.0
1.5
1.0
0.5
ΔV (% of V$_{oc(STC)}$)
10^{-4}
10^{-3}
10^{-2}
10^{-1}
10^{0}
T$_a$ (s)
99.9
99.7
99.5
99.3
99.1
98.9
98.7
98.5
98.3
98.1
Efficiency

(c)

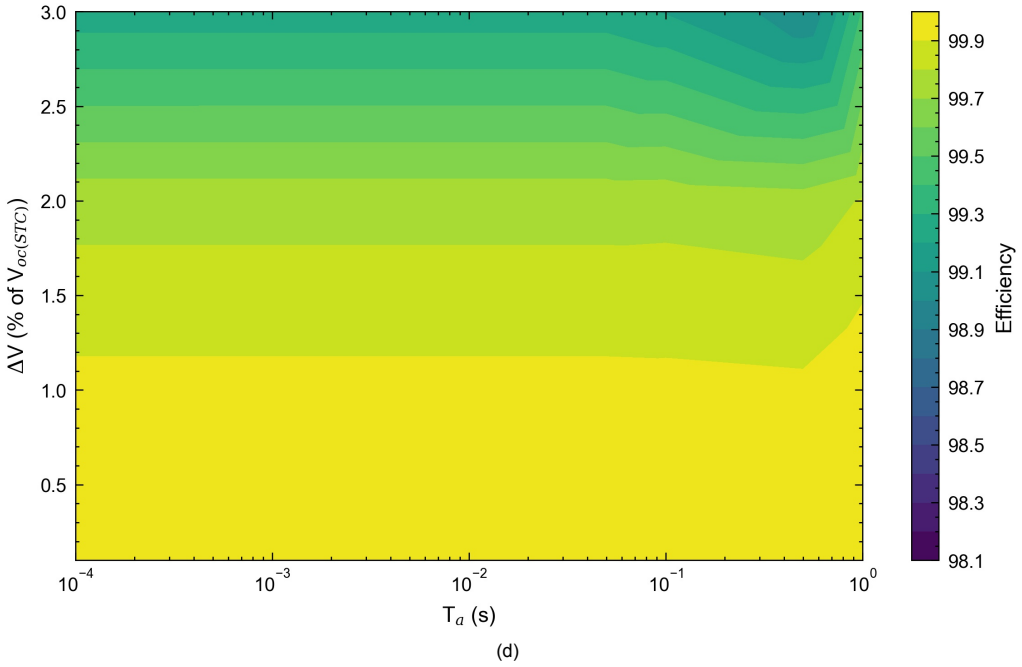

(d)

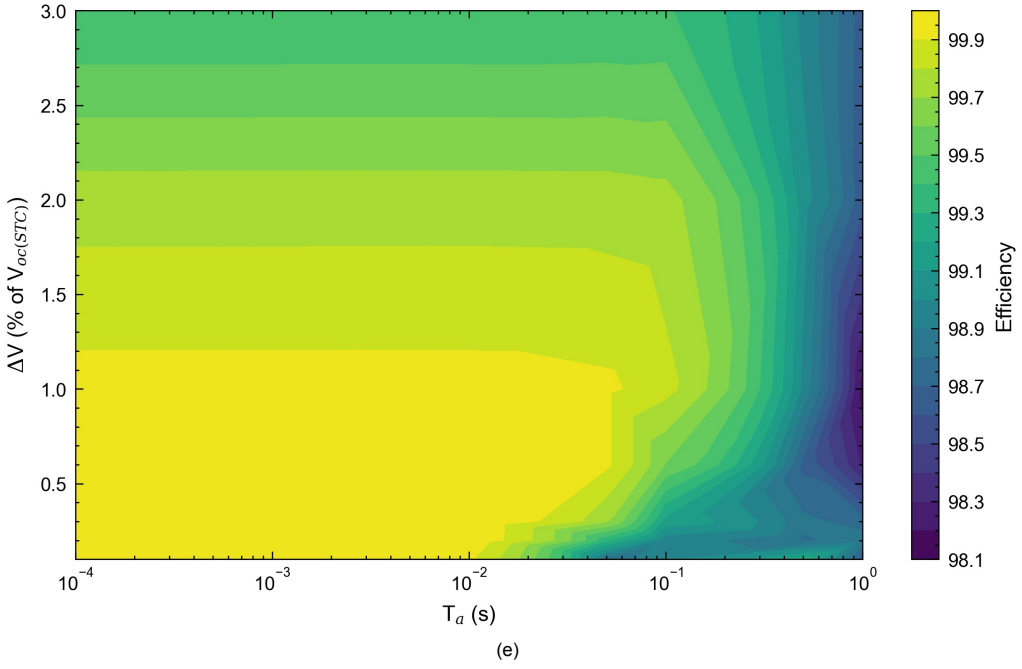

(e)

Figure 4.12: Average hourly P&O efficiency depending on perturbation step amplitude (ΔV) and sampling interval T_a during a (a) clear hour and (b) overcast hour (c) mildly variable hour (d) moderately variable hour and (e) highly variable hour

5 Discussion

In this chapter, the most important observations found throughout the process of this project are presented. The observations entail conclusions made from the data exploratory analysis was discussed in Chapter 4 as well as other general notes. Firstly, ideas behind the importance of temporal resolution in context of P&O efficiency studies are presented in Section 5.1. Then the chapter moves on to explain mathematical meaning of efficiency calculations and interpretation of efficiency values in Section 5.2. This chapter aims to provide more insight into the results and proposes points of view to the P&O efficiency topic that could be essential to consider when researching P&O efficiency.

5.1 Temporal resolution and P&O efficiency

Temporal resolution has been mentioned throughout the report multiple times. It is one of the most important factors to consider when examining both P&O efficiency and irradiance variability. The smoothing effect of averaging reduces informativeness of irradiance data. Using irradiance data averaged over a long period of time complicates investigations of P&O operation. This is because the algorithm perturbs voltage much more frequently and estimation of irradiance values between the data points is necessary. Furthermore, the loss of information when averaging greatly affects the values variability quantifiers have which must be considered when comparing irradiance conditions between one case and another. Lastly, even P&O efficiency acquirers different values depending on what temporal scale efficiency is presented.

As discussed in Section 2.3, the P&O algorithm perturbs voltage every sampling period T_a which is one of the two P&O parameters. In this project, the dataset was sampled at 3 s intervals whereas the T_a for the majority of the analysis was considered to be 0.5 ms. To apply the methodology proposed in Chapter 3, calculations of P&O efficiency required a data point of irradiance every sampling period of the P&O algorithm. For this, a linear increase/decrease between two subsequent irradiance data samples was assumed and 59 additional irradiance values were added. Number of such approximated points is determined by the ratio of T_a and irradiance data sampling period and the more points are created artificially the less accurate modelling becomes. To that end, it is essential to obtain high-resolution irradiance data so the ratio is kept low or improving the assumptions on which additional data points are generated. The latter could be done by implementing irradiance downscaling models. Dirichlet downscaling model proposed by Firmane et al. [28] was tested (but not used) during this project. Usually such downscaling models are implemented to downsample irradiance data from hours or tens of minutes to 1 min scale. However, as this study is concerned with frequently perturbing algorithm a downscaling from 1 min to 3 s resolution was attempted. Example of the results can be seen in Figure 5.1. Values of generated irradiance data seem to be very similar to the measured ones however validation of results is required. Nevertheless, Dirichlet downsampling model seems to be effective. It could produce a more accurate estimation than linear interpolation when estimating data poits between every 1 min at 3 s intervals (and most likely even on smaller scales like 1 s to 0.2 ms). Hence, use of this downsampling model could assist when studying processes under variable irradiance conditions and should be further explored.

Loss of variance of irradiance values was discussed in Section 2.5 and illustrated in Figure 2.13. Additionally, in Figure 2.12 maximum irradiance ramp rate is found to be 200 W/m^2/s when irradiance data are sampled every 5 s, whereas results produced using 3 s data and presented in this thesis

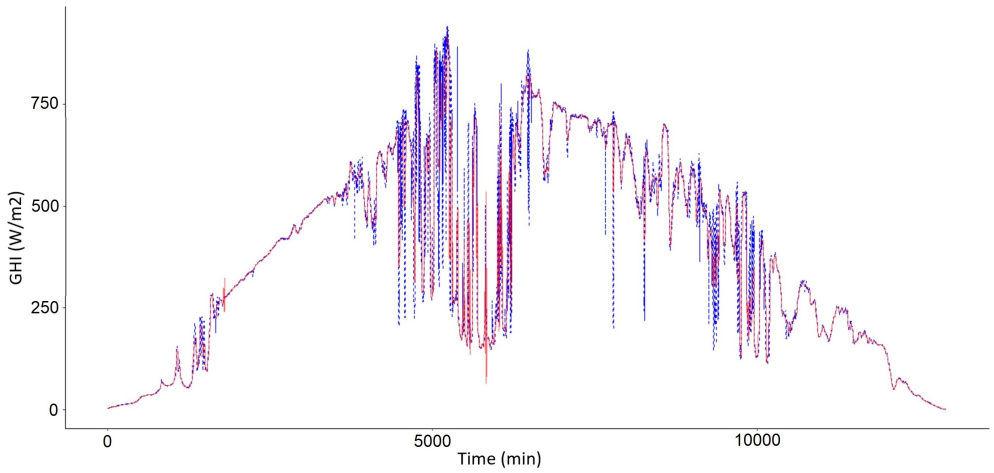

Figure 5.1: Measured (blue dashed line) and generated using Dirichlet downscaling model (red) 3 s irradiance time series

indicate ramp rates of 300 W/m^2/s. However, from these examples, it is difficult to really understand how much variability in the irradiance curve is smoothed. Therefore, for purpose of discussion, metrics quantifying irradiance variability that was used in relation to P&O efficiency were recomputed for the whole year using irradiance data averaged for different sampling periods (3 s, 5 s, 10 s, 30 s, 1 min, 5 min, 10 min, 30 min and 60 min). As can be seen in Figure 5.2, on a logarithmic sampling period scale there is an exponential decrease of all variability metrics but mean ramp rate which stays relatively constant. Interestingly, even VI magnitudes reduce with a similar trend as the other metrics even though its amplitude depends on data resolution as well as the variance of irradiance values. This figure is proposed as an example of quantification of averaging smoothing effects, however, generalization capabilities of it should be tested using year's irradiance data from other locations. Nevertheless, the effects are evident and must be considered for any study that investigates PV power plant operation and performance with regards to variability.

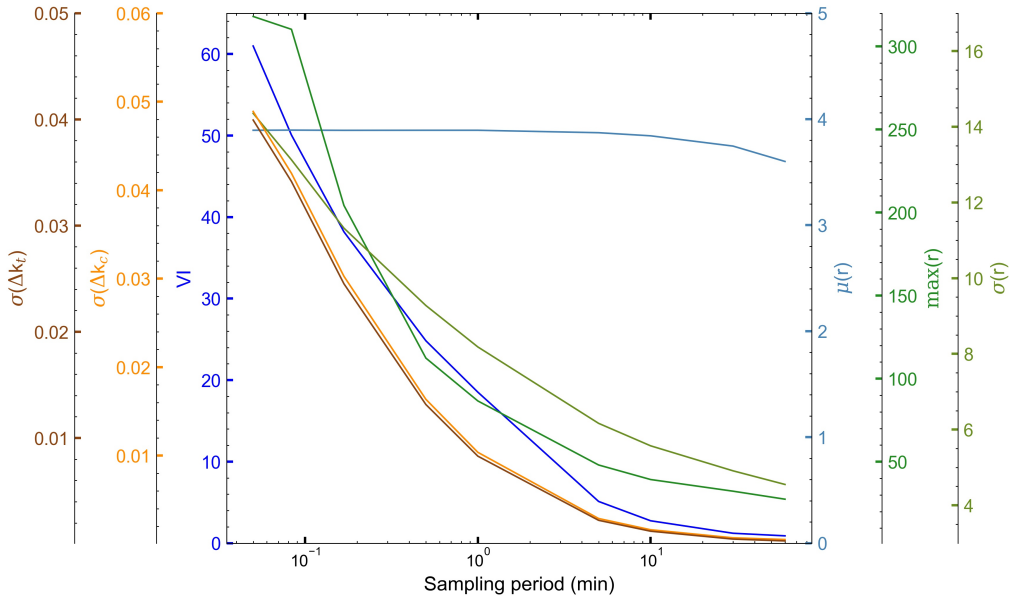

Figure 5.2: Data resolution effect on magnitude of variability measures

Lastly, when exploring the results of the dataset prepared by methodology described in Chapter 3 there was an evident variation of efficiency values averaged for different time periods as well. In Section 4.2 mean efficiency for a year was found to be 99.93 %, monthly efficiencies to have values

above 99.9 % and daily - above 99.82 % whereas Figure 4.2 reports efficiencies to be mostly above 95 %. However, comparison of these observations is limited and hence a more thorough investigation is proposed. Figure 5.3 shows box plots of efficiency values averaged from 3 s up to 1 month. It must be noted, that with increasing averaging intervals the number of efficiency data points decreases. The figure shows decreasing median values when data are averaged over longer periods of time. However, the number of outliers in 3 s efficiency is tremendous. At each increasing interval more and more of the outliers are averaged to the mean values and the interquartile range increases and shifts to lower magnitudes. When looking at 1 day period almost no outliers are present and when averaged into months interquartile range shrinks while still decreasing in median value. From this, it is judged that comparison of efficiency values on different time scales is difficult as the efficiency is more unpredictable when values are averaged for shorter time periods. However, it is certain that the minimum efficiency value that could be expected when studying P&O efficiency at small time scales is lower than the minimum at monthly intervals.

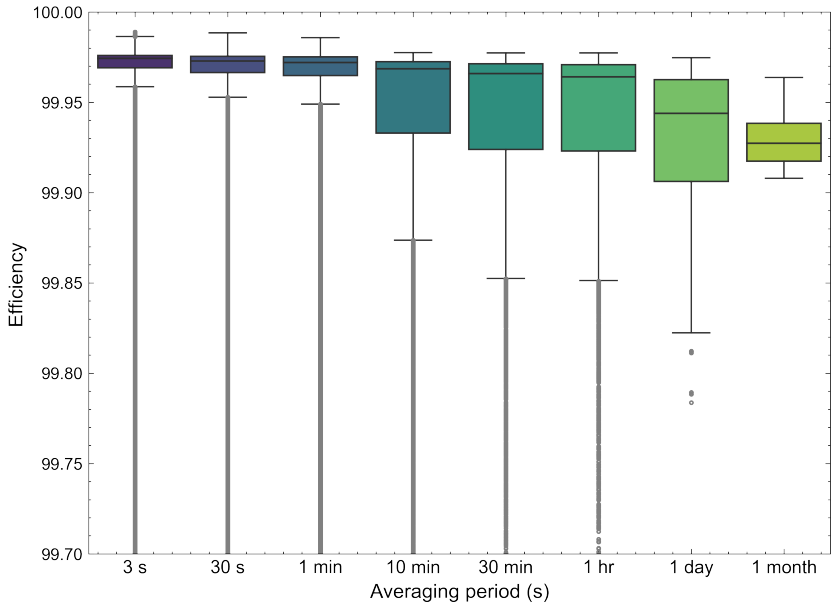

Figure 5.3: P&O efficiency values when averaged for different time periods

5.2 Comparison of P&O efficiency values

During the process of this project, another observation was made. As discussed in Section 2.1, at higher irradiance the maximum power increases and P-V curves extend to higher amplitudes. This means that the same change in voltage results in a higher change of power. This means that operating point will diverge more from the MPP which would indicate worse performance than in lower irradiance levels. However, this is not exactly the case. In Figure 2.11a efficiency values are higher at higher irradiance levels. The authors of the figure argued that this is dependant on converter characteristics. However, this thesis did not assume any physical parameters of a converter but reduced efficiency at lower irradiance amplitude was also observed. As an example, Figure 5.4 shows boxplots of 3s P&O efficiency versus 3s ramp rates with 3 irradiance levels that the ramp ends: low (<400 W/m^2/s), medium (400-800 W/m^2/s) and high (>800 W/m^2/s). Here it is observed that at the same range of ramp rates but higher irradiance, efficiency will most likely be higher.

This work proposes a point of view to explain such interesting behaviour by inspecting the meaning behind efficiency calculations. Figure 5.5 illustrates a simplified example of this meaning. Assuming that both MPP and P&O power at instance j is lower in amplitude than at instance i, the instantaneous efficiency can be higher at instance i even if the difference in power ΔP at this moment is larger than in instance j. Or, looking from another perspective, efficiency at larger power (and irradiance) values

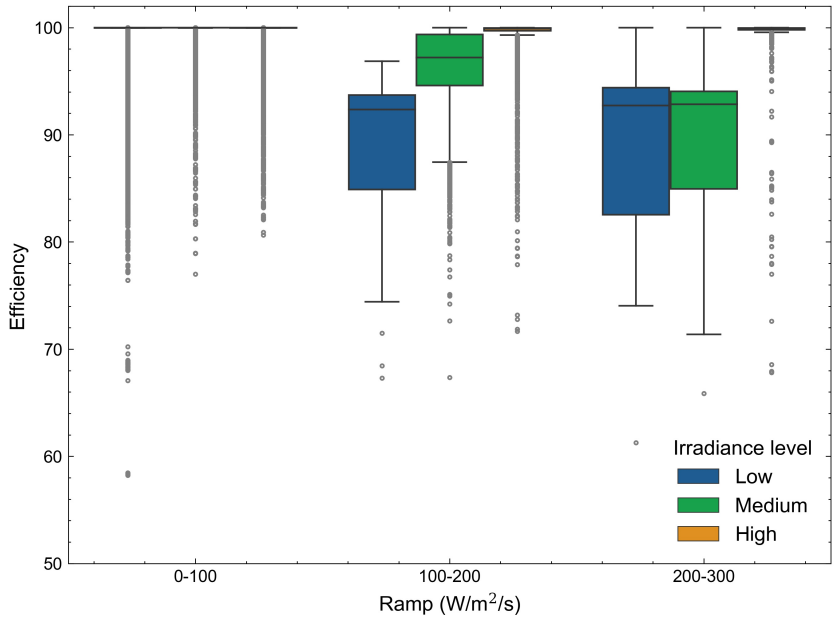

Figure 5.4: P&O efficiency in different ramping events segregated by irradiance level

will be greater than at lower power even if the power loss ΔP is the same. The severity of this effect on instantaneous efficiency values calculated using real irradiance data is unknown and should be investigated further. If the effect is substantial a different metric for measuring performance in different irradiance amplitudes could be proposed; the metrics could include irradiance weighted efficiency or weighted power difference. However, the meaning of efficiency values should be kept in mind when comparing values observed in two separate instances when irradiance conditions are different.

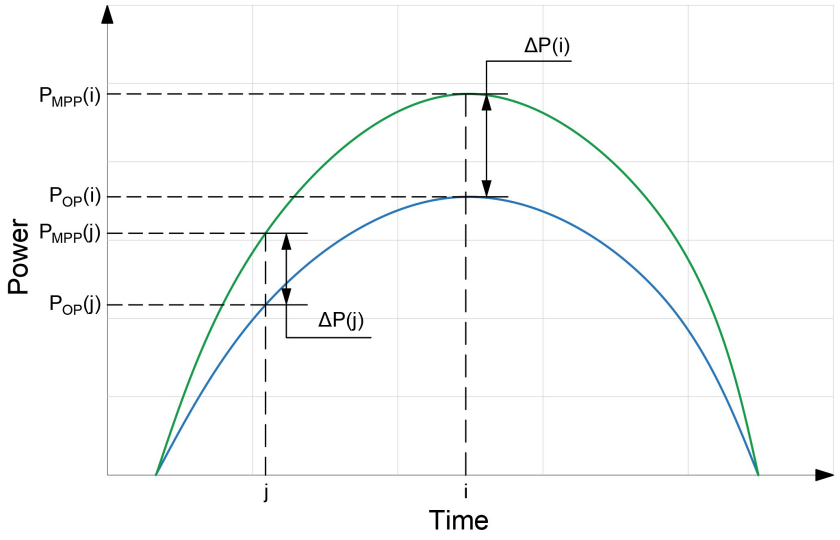

Figure 5.5: P&O efficiency values when averaged for different time periods

6

Conclusion & Recommendations

With the urgency of climate change issues, solar PV energy systems global installed capacity is rapidly growing. Because such installations require extensive resources, it is essential that their efficiency is high. MPPT is a very important and integral part of a PV system which ensures that the power drawn from the PV module is at maximum. Therefore, proper MPPT performance is of vital importance. MPPT is realised through the use of an algorithm that controls a DC-DC converter that can change the operating power point of the system. The most widely used algorithm due to its simplicity and cost of implementation is P&O algorithm. However, it has drawbacks as well: in steady-state conditions P&O algorithm makes the OP to oscillate around MPP, and in dynamic conditions, it suffers from slow response and confusion. While the severity of these downsides are dependant on the P&O algorithm parameters sampling interval T_a and perturbation amplitude ΔV, conditions in which the algorithm operates are determined by irradiance variability.

While there are numerous studies found in literature on P&O efficiency and irradiance variability separately, the link between the two topics has not been explored. Hence, this thesis aims to bridge this gap. Most of the P&O efficiency studies are performed experimentally. However, analysis in this work is carried out using real 3 s irradiance data, modelling the corresponding PV power output and determining the operating point of the system by implemented P&O algorithm without assuming any physical behaviour of a converter. Then, using OP and MPP power values, 3 s averages of P&O efficiency are obtained and variability metrics are calculated from irradiance data. Finally, exploratory analysis of the produced dataset is carried out to answer the main research question which asks:

How does efficiency of maximum power point tracking P&O algorithm vary when exposed to different conditions of irradiance variability?

To answer the main research question the following sub-questions are elaborated upon:

- *Is there variation in daily and monthly efficiency of P&O algorithm, and if there is how can such variation be explained?*

Section 4.2 presented results of the daily and larger scales. Using irradiance data sampled every 3 s from Oahu, Hawaii and P&O parameters $T_a = 50ms$ and $\Delta V = 0.6\%$ of $V_{oc(STC)}$, average P&O efficiency during a year was determined to be 99.93 %. Monthly efficiencies show minor variations in amplitude, with winter months having the largest efficiencies. This was explained by deterministically classifying each day of the year by its variability to five classes: high, moderate, mild, clear and overcast. The number of days in each class was counted for every month and December, January and February showed the lowest counts of highly variable days and largest counts of clear and overcast days. This also indicates that efficiency is indeed affected by variability of irradiance. Additionally, average daily efficiencies were inspected depending on the class of the day. The results showed a variation of efficiency values range between days with high variability days having the lowest efficiency while clear days have the highest. Magnitudes of daily efficiencies exceed 99.8 %.

- *How can variability be quantified? How do these quantities relate to efficiency?*

There are a number of metrics proposed in literature that can quantify variability. Such metrics can be classified as statistical, deterministic or probabilistic. In this research one deterministic metric (VI) and six statistical features of irradiance ($\sigma(\Delta k_c)$,$\sigma(\Delta k_t)$, σ(r), min(r) and max(r) and μ(r)) are used. As variability quantifiers describe a period of time, the selected metrics are calculated for 1 min periods

using 3 s data. Efficiency is aggregated by averaging for 1 min to match the metrics' resolution. The full year 1 min dataset features are then analysed against each other using Pearson correlation factors. However, because of the major scatter of 1 min data, Pearson correlation between variability metrics and efficiency is found weak. To that end, this work proposes using average 1 min values within bins of variability metric, this way the scattering is reduced. A general decrease of efficiency average in each bin is observed with increasing values of variability metrics. Additionally, a polynomial line fits are performed with which efficiency can be approximated when variability is known. Coefficients and goodness-of-fit metrics are provided.

- *Does P&O parameter tuning have influence on P&O efficiency? How does that depend on irradiance variability?*

There is a range of P&O parameter values mentioned in literature. However, the selection of the parameter pair is very important but not straightforward. To that end, a sensitivity study is performed that inspects the effect of varying sampling intervals and perturbation amplitudes in five different cases of variability on mean hourly efficiency. It has shown that in mild, moderate variability, clear and overcast hours efficiency is mostly dependant on ΔV which can be explained by OP oscillations around MPP as smaller perturbation steps results in smaller deviations from maximum power. However, in high variability hour large T_a results in low efficiency especially when paired together with ΔV of 1 % of $V_{oc(STC)}$. In general, efficiency is more sensitive to its parameters when variability is high. Lastly, it is concluded that regardless of variability level high efficiency will be obtained if ΔV is less than 1 % of $V_{oc(STC)}$ and T_a below 10 ms, however, transient behaviour of the converter should be considered.

This work also provides a discussion about general observations made throughout the project. Firstly, the importance of considering temporal resolution in variability and efficiency studies is highlighted. To accurately determine operating power governed by P&O algorithm, irradiance data resolution and P&O sampling interval ratio should be minimal. For this, data should be sampled at smaller periods. Another way to solve this issue is to estimate irradiance values between sampled data points using a downsampling model. Another problem related to irradiance data sampling interval is the loss of variability evident within the irradiance dataset due to averaging effect. For a better understanding of this effect, a figure showing values and trends of variability metrics at increasing data sampling period is provided. Efficiency magnitudes also change when they are averaged for different time spans. While the explanation of these changes involves understanding the distribution of efficiency values, it concludes that the minimum efficiency that could be observed when inspecting values at different scales is smallest when efficiency is averaged for the shortest period of time. Additionally, another observation was made that indicates a potential reason for higher efficiency values at higher irradiance values. This observation entails mathematical meaning of efficiency calculations where two instances that have the same difference in power will have different efficiencies because of the difference in power amplitudes in each instance which is caused by different irradiance levels.

From the results and discussion following recommendations for further research and improvement of the established methodology are proposed:

- Utilization of Dirichlet downscaling algorithm for estimations of high-resolution irradiance changes from obtained irradiance data at minutely scale.
- Investigation of mathematical meaning of efficiency calculations in terms of its capability to describe P&O performance and efficiency comparability at different irradiance levels.
- Examining the reasons behind scattering of high-resolution efficiency values raising the question: why are there different values of efficiency observed at the same quantified variability.
- Inclusion of partial shading in P&O efficiency during different irradiance variability studies.
- Studying efficiency performance when both irradiance and temperature is variable.
- Use of a more complex and accurate temperature model for PV output estimations.
- Computations of PV module output I-V curves using a more elaborate and precise model.
- Implementing a more robust variability classification method that could classify time periods using high temporal resolution irradiance data.

A

ESRA model

To estimate global horizontal clear-sky irradiance ESRA model firsts determines its direct and diffuse components as explained further [46]. The direct (or beam) clear-sky irradiance on a horizontal surface is given by Equation A.1

$$B_c = I_0 * \varepsilon * \sin(\theta_{El}) * \exp\left(-0.8662 * T_{\mathrm{L}}(\mathrm{AM2}) * m * \delta_{\mathrm{R}}(m)\right) \tag{A.1}$$

where I_0 is the solar constant - normal extraterrestrial irradiance, equal to 1367 W/m^2; ε is correction for variation of Sun to Earth distance from the mean value (calculated using Equation A.2); $T_{\mathrm{L}}(\mathrm{AM2})$ is Linke turbidity factor under air mass equal to 2; m is relative optical air mass and $\delta_{\mathrm{R}}(m)$ is integral Rayleigh optical thickness.

$$\varepsilon = \frac{1}{[1.0014 - 0.01671\cos(g) - 0.00014\cos(2g)]^2} \tag{A.2}$$

where g is the mean anomaly and is equal to $357.529 + 0.98560028 * DOY$.

Relative optical air mass is a measure of optical path length for irradiance to traverse through the atmosphere [38]. This relative distance must be corrected to account for the air mass pressure by considering the site elevation above sea level z. In Oahu elevation was determined to be 6 m above sea level. In this work, relative air mass is computed as given in Equations A.3 and A.4:

$$m = \frac{1}{sin(\theta_{El}') + 0.50572(\theta_{El}' + 6.07995)^{-1.6364}} \tag{A.3}$$

$$\theta_{El}' = \theta_{El} + 0.061359\frac{180}{\pi}\left(\frac{0.1594 + 1.1230\frac{\pi}{180} * \theta_{El} + 0.065656 * \left(\frac{\pi}{180}\right)^2 * \theta_{El}^2}{1 + 28.9344\frac{\pi}{180} * \theta_{El} + 277.3971 * \left(\frac{\pi}{180}\right)^2 * \theta_{El}^2}\right) \tag{A.4}$$

Integral Rayleigh optical thickness is the spectrally integrated optical thickness of the Rayleigh (clean and dry) atmosphere at standard conditions [47]. The thickness is calculated for a specified path length and hence depend the relative optical air mass m as follows:

$$\begin{cases} \text{if } m \leq 20 \\ \quad 1/\delta_{\mathrm{R}}(m) = 6.62960 + 1.75130m - 0.12020m^2 + 0.00650m^3 - 0.00013m^4 \\ \text{if } m > 20 \\ \quad 1/\delta_{\mathrm{R}}(m) = 10.4 + 0.718m \end{cases} \tag{A.5}$$

Once all the required values of correction for variation of Sun to Earth distance, optical air mass and integral Rayleigh optical thickness is obtained and beam clear-sky irradiance component is calculated, the model moves on to compute the diffuse component as given in Equation A.6:

$$D_c = I_0 * \varepsilon * T_{\mathrm{rd}}\left(T_{\mathrm{L}}(\mathrm{AM2})\right) * F_{\mathrm{d}}\left(\theta_{El}, T_{\mathrm{L}}(\mathrm{AM2})\right) \tag{A.6}$$

where $T_{\mathrm{rd}}\left(T_{\mathrm{L}}(\mathrm{AM2})\right)$ is the diffuse transmission function at zenith - when the sun elevation is equal to 90°:

$$T_{\mathrm{rd}}\left(T_{\mathrm{L}}(\mathrm{AM2})\right) = -1.5843 \times 10^{-2} + 3.0543 \times 10^{-2} T_{\mathrm{L}}(\mathrm{AM2}) + 3.797 \times 10^{-4}\left[T_{\mathrm{L}}(\mathrm{AM2})\right]^2 \tag{A.7}$$

and $F_{\mathrm{d}}\left(\theta_{El}, T_{\mathrm{L}}(\mathrm{AM2})\right)$ is the diffuse angular function given by:

$$F_{\mathrm{d}}\left(\theta_{El}, T_{\mathrm{L}}(\mathrm{AM2})\right) = A_0 + A_1 \sin\left(\theta_{El}\right) + A_2 \left[\sin\left(\theta_{El}\right)\right]^2 \tag{A.8}$$

where A_0, A_1 and A_2 depend on Linke turbidity factor and are obtained using Equation A.9:

$$\begin{cases} A_0 = 2.6463 \times 10^{-1} - 6.1581 \times 10^{-2} T_L(\mathrm{AM2}) + 3.1408 \times 10^{-3} \left[T_{\mathrm{L}}(\mathrm{AM2})\right]^2 \\ A_1 = 2.0402 + 1.8945 \times 10^{-2} T_{\mathrm{L}}(\mathrm{AM2}) - 1.1161 \times 10^{-2} \left[T_{\mathrm{L}}(\mathrm{AM2})\right]^2 \\ A_2 = -1.3025 + 3.9231 \times 10^{-2} T_{\mathrm{L}}(\mathrm{AM2}) + 8.5079 \times 10^{-3} \left[T_{\mathrm{L}}(\mathrm{AM2})\right]^2 \end{cases} \tag{A.9}$$

with condition for A_0:

$$\text{if } \left(A_0 \cdot T_{\mathrm{rd}}\right) < 2 \times 10^{-3}, A_0 = 2 \times 10^{-3} / T_{\mathrm{rd}} \tag{A.10}$$

Lastly, the global horizontal clear-sky irradiance is obtained by summing direct and diffuse components:

$$G_c = B_c + D_c \tag{A.11}$$

Bibliography

[1] United States Environmental Protection Agency. Global greenhouse gas emissions data. https://www.epa.gov/ghgemissions/global-greenhouse-gas-emissions-data.

[2] European Environmental Agency. Energy and climate change, 2021. https://www.eea.europa.eu/signals/signals-2017/articles/energy-and-climate-change.

[3] International Energy Agency. Data & Statistics: Total energy supply (TES) by source (World), 2020. https://www.iea.org/data-and-statistics/data-browser?country=WORLD&fuel=Energysupply&indicator=TPESbySource.

[4] International Environmental Agency. Renewable energy market update 2021, 2021. https://www.iea.org/reports/renewable-energy-market-update-2021.

[5] LONGi. LONGi sets another new world record for module efficiency, 2020. http://www.en.longi-solar.com/home/events/press_detail/id/184_LONGi_sets_another_new_world_record_for_module_efficiency.html.

[6] Kashif Ishaque, Zainal Salam, and George Lauss. The performance of perturb and observe and incremental conductance maximum power point tracking method under dynamic weather conditions. *Applied Energy*, 119:228–236, 2014.

[7] Nabil Karami, Nazih Moubayed, and Rachid Outbib. General review and classification of different MPPT techniques. *Renewable and Sustainable Energy Reviews*, 68:1–18, 2017.

[8] Nicola Femia, Giovanni Petrone, Giovanni Spagnuolo, and Massimo Vitelli. Optimization of perturb and observe maximum power point tracking method. *IEEE transactions on power electronics*, 20(4):963–973, 2005.

[9] Trishan Esram and Patrick L. Chapman. Comparison of photovoltaic array maximum power point tracking techniques. *IEEE Transactions on energy conversion*, 22(2):439–449, 2007.

[10] Robert Blaga and Marius Paulescu. Quantifiers for the solar irradiance variability: A new perspective. *Solar Energy*, 174:606–616, 2018.

[11] Armando Castillejo-Cuberos and Rodrigo Escobar. Understanding solar resource variability: An in-depth analysis, using chile as a case of study. *Renewable and Sustainable Energy Reviews*, 120:109664, 2020.

[12] Gerald M. Lohmann. Irradiance variability quantification and small-scale averaging in space and time: A short review. *Atmosphere*, 9(7):264, 2018.

[13] Arno Smets, Klaus Jäger, Olindo Isabella, René van Swaaij, and Miro Zeman. *Solar Energy: The physics and engineering of photovoltaic conversion, technologies and systems*. UIT Cambridge Limited, 2016.

[14] Alivarani Mohapatra, Byamakesh Nayak, Priti Das, and Kanungo Barada Mohanty. A review on MPPT techniques of PV system under partial shading condition. *Renewable and Sustainable Energy Reviews*, 80:854–867, 2017.

[15] Ned Mohan, Tore M. Undeland, and William P. Robbins. *Power electronics: converters, applications, and design*. John Wiley & Sons, 2nd edition, 2003.

[16] Roberto Faranda and Sonia Leva. Energy comparison of MPPT techniques for PV systems. *WSEAS transactions on power systems*, 3(6):446–455, 2008.

[17] Ali M. Eltamaly and Almoataz Y. Abdelaziz. *Modern maximum power point tracking techniques for photovoltaic energy systems*. Springer, 2019.

[18] D.P. Hohm and M.E. Ropp. Comparative study of maximum power point tracking algorithms. *Progress in photovoltaics: Research and Applications*, 11(1):47–62, 2003.

[19] Moacyr Aureliano Gomes De Brito, Luigi Galotto, Leonardo Poltronieri Sampaio, Guilherme de Azevedo e Melo, and Carlos Alberto Canesin. Evaluation of the main MPPT techniques for photovoltaic applications. *IEEE transactions on industrial electronics*, 60(3):1156–1167, 2012.

[20] Ke Yan, Yang Du, and Zixiao Ren. MPPT perturbation optimization of photovoltaic power systems based on solar irradiance data classification. *IEEE transactions on sustainable energy*, 10(2):514–521, 2018.

[21] Ashish Pandey, Nivedita Dasgupta, and Ashok Kumar Mukerjee. High-performance algorithms for drift avoidance and fast tracking in solar MPPT system. *IEEE Transactions on Energy conversion*, 23(2):681–689, 2008.

[22] Nafaa Jeddi and Lilia El Amraoui Ouni. Comparative study of MPPT techniques for PV control systems. In *2014 International Conference on Electrical Sciences and Technologies in Maghreb (CISTEM)*, pages 1–7. IEEE, 2014.

[23] R. Bründlinger, N. Henze, H. Häberlin, B. Burger, A. Bergmann, and F. Baumgartner. prEN 50530-The new european standard for performance characterisation of PV inverters. In *24th EU PV Conf., Hamburg, Germany*, 2009.

[24] Maciej Piotrowicz and Witold Marańda. Report on efficiency of field-installed PV-inverter with focus on radiation variability. In *Proceedings of the 20th International Conference Mixed Design of Integrated Circuits and Systems-MIXDES 2013*, pages 440–443. IEEE, 2013.

[25] Meteotest AG. Meteonorm 8, 2021. https://meteonorm.com/en/.

[26] EU SCIENCE HUB. Photovoltaic geographical information system (PVGIS), 2021. https://ec.europa.eu/jrc/en/pvgis.

[27] Joakim Widén and Joakim Munkhammar. Spatio-temporal downscaling of hourly solar irradiance data using gaussian copulas. In *2019 IEEE 46th Photovoltaic Specialists Conference (PVSC)*, pages 3172–3178. IEEE, 2019.

[28] Âzeddine Frimane, Jamie M. Bright, Dazhi Yang, Badr Ouhammou, and Mohammed Aggour. Dirichlet downscaling model for synthetic solar irradiance time series. *Journal of Renewable and Sustainable Energy*, 12(6):063702, 2020.

[29] World Radiation Monitoring Center. Baseline surface radiation network, 2019. https://bsrn.awi.de/.

[30] Joshua Stein, Clifford Hansen, and Matthew J. Reno. The variability index: A new and novel metric for quantifying irradiance and PV output variability. Technical report, Sandia National Laboratories, 2012.

[31] M. Sengupta and A. Andreas. Oahu solar measurement grid (1-year archive): 1-second solar irradiance; Oahu, Hawaii (data). Technical report, National Renewable Energy Lab.(NREL), Golden, CO (United States), 2010. NREL Report No. DA-5500-56506. http://dx.doi.org/10.5439/1052451.

[32] Markus Kottek, Jürgen Grieser, Christoph Beck, Bruno Rudolf, and Franz Rubel. World map of the Köppen-Geiger climate classification updated. 2006.

[33] Muhammad Iqbal. *An introduction to solar radiation*. Academic Press, Inc., London, UK, 1983.

[34] S.C. Bhatia. *Advanced Renewable Energy Systems*, chapter 2 - Solar radiations, pages 32–67. CRC Press, Woodhead Publishing India, Florida, U.S., New Delhi, India, 2014.

[35] Ibrahim Reda and Afshin Andreas. Solar position algorithm for solar radiation applications. *Solar energy*, 76(5):577–589, 2004.

[36] Joshua S. Stein, William F. Holmgren, Jessica Forbess, and Clifford W. Hansen. PVLIB: Open source photovoltaic performance modeling functions for Matlab and Python. In *2016 IEEE 43rd photovoltaic specialists conference (PVSC)*, pages 3425–3430. IEEE, 2016.

[37] NA Engerer and FP Mills. Kpv: A clear-sky index for photovoltaics. *Solar energy*, 105:679–693, 2014.

[38] F. Antonanzas-Torres, R. Urraca, J. Polo, O. Perpiñán-Lamigueiro, and R. Escobar. Clear sky solar irradiance models: A review of seventy models. *Renewable and Sustainable Energy Reviews*, 107:374–387, 2019.

[39] Jan Remund, Lucien Wald, Mireille Lefèvre, Thierry Ranchin, and John Page. Worldwide Linke turbidity information. In *ISES Solar World Congress 2003*, volume 400, pages 13–p. International Solar Energy Society (ISES), 2003.

[40] HOMER Energy LLC. HOMER Pro: How HOMER calculates clearness index, 2021. https://www.homerenergy.com/products/pro/docs/latest/how_homer_calculates_clearness_index.html.

[41] Sandia module temperature model. https://pvpmc.sandia.gov/modeling-steps/2-dc-module-iv/module-temperature/sandia-module-temperature-model/.

[42] Wenqi Zhang, William Kleiber, Anthony R Florita, Bri-Mathias Hodge, and Barry Mather. A stochastic downscaling approach for generating high-frequency solar irradiance scenarios. *Solar Energy*, 176:370–379, 2018.

[43] Filippo Spertino, Jawad Ahmad, Paolo Di Leo, and Alessandro Ciocia. A method for obtaining the IV curve of photovoltaic arrays from module voltages and its applications for MPP tracking. *Solar Energy*, 139:489–505, 2016.

[44] Bálint Hartmann. Comparing various solar irradiance categorization methods–A critique on robustness. *Renewable Energy*, 154:661–671, 2020.

[45] Jinwook Seo and Ben Shneiderman. A rank-by-feature framework for unsupervised multidimensional data exploration using low dimensional projections. In *IEEE Symposium on Information Visualization*, pages 65–72. IEEE, 2004.

[46] Christelle Rigollier, Olivier Bauer, and Lucien Wald. On the clear sky model of the ESRA—European Solar Radiation Atlas—with respect to the Heliosat method. *Solar energy*, 68(1):33–48, 2000.

[47] F. Kasten. The Linke turbidity factor based on improved values of the integral Rayleigh optical thickness. *Solar energy*, 56(3):239–244, 1996.